Active Reconfigurable Intelligent Surface-Assisted MISO Integrated Sensing and Communication Systems for Secure Operation

A. Abdelaziz Salem , Mahmoud H. Ismail, Senior Member, IEEE, and Ahmed S. Ibrahim, Member, IEEE

Abstract—Spectrum congestion has motivated the recent introduction of integrated sensing and communication (ISAC) systems where radar and communications functionalities co-exist and share the same spectrum. This is accompanied by extensive research in the area of reconfigurable intelligent surfaces (RIS), thanks to their ability to improve the ISAC systems. In this paper, the physical layer security of a multiuser multiple-input single-output (MU-MISO) ISAC system is investigated when the system is subject to eavesdropping by a malicious unmanned aerial vehicle (UAV). In particular, we propose using an active RIS to maximize the achievable secrecy rate of the system through jointly designing the radar receive beamformers, the active RIS reflection coefficients matrix and the transmit beamformers at the dual-function base station of the ISAC system. This is done while taking into account a minimum radar detection signal-to-noise ratio (SNR) and total system power budget constraints. The resulting non-convex optimization problem is tackled by exploiting fractional programming (FP) and majorization-minimization (MM) techniques to achieve a solution. Our numerical results show the superiority of active RIS to achieve the goal when compared with passive RIS or with an ISAC without an RIS. Results also show that passive RIS could still be a viable solution to achieve this goal but at the expense of a much larger needed size especially when lower power budgets are available.

Index Terms—Active reconfigurable intelligent surfaces (RIS), alternating optimization, Integrated sensing and communication (ISAC), multiuser multi-input single-output (MU-MISO), physical layer security (PLS).

Manuscript received 24 August 2022; revised 8 November 2022; accepted 1 December 2022. Date of publication 7 December 2022; date of current version 18 April 2023. The work of A. Abdelaziz Salem and Mahmoud H. Ismail was supported by the American University of Sharjah through Faculty Research under Grants FRG20-M-E10 and FRG22-C-E13. The work of Ahmed S. Ibrahim was supported by the National Science Foundation under Award CNS-1816112. The review of this article was coordinated by Dr. Chau Yuen. (Corresponding author: Mahmoud H. Ismail.)

A. Abdelaziz Salem is with the Department of Electrical Engineering, American University of Sharjah, Sharjah 26666, UAE, and also with the Department of Electronics and Electrical Communications Engineering, Faculty of Electronic Engineering, Menoufia University, Menoufia 32952, Egypt (e-mail: ahmed.abdalaziz40@el-eng.menofia.edu.eg).

Mahmoud H. Ismail is with the Department of Electrical Engineering, American University of Sharjah, Sharjah 26666, UAE, and also with the Department of Electronics and Communications Engineering, Faculty of Engineering, Cairo University, Giza 12613, Egypt (e-mail: mhibrahim@aus.edu).

Ahmed S. Ibrahim is with the Electrical and Computer Engineering Department, Florida International University, Miami, FL 33174 USA (e-mail: aibrahim@fiu.edu).

Digital Object Identifier 10.1109/TVT.2022.3227319

I. INTRODUCTION

ITH a plethora of industrial applications, devices and services, the next generation of wireless networks (beyond 5G- B5G) will be prone to spectrum congestion. It is estimated that the number of connected devices worldwide will grow to about 75 billions by 2025 [1], which emphasizes the impending demand for communications resources. As a consequence, there has been great interest in enabling integrated sensing and communication (ISAC) systems, also referred to as dual functional radar and communication (DFRC), as a possible solution for the communications-radar spectrum co-existence challenge [2], [3], [4]. Additionally, ISAC systems could be used in multiple emerging applications such as location awareness [5], area imaging and unmanned aerial vehicles (UAVs) monitoring [6].

Enabling interference-aware radar-communication coexistence, which is one of the fundamental challenges in ISAC, was recently addressed in the literature (e.g., [7], [8], [9]). For example, designing unified beamformers for the joint transmission of communication and radar sensing signals was introduced in [8], [9], [10], [11], [12]. Furthermore, employing passive reconfigurable intelligent surfaces (RIS)¹ in ISAC systems was shown to extend their coverage. More specifically, through optimizing the RIS phase shifts of such RIS-assisted ISAC systems, or for brevity RIS-ISAC, coverage extension was accomplished. Beyond passive RIS, active RIS can provide further gain through amplification of the reflected signals [17].

A. Literature Review: RIS-Assisted ISAC Systems

An RIS is a programmable low-complex meta-surface, which consists of an array of passive elements being manipulated with certain phase shifts to control the reflection of incident radio waves [15], [16]. Specifically, the wireless environment can be dynamically adjusted in real time to enhance reliability of sensing, increase communication rate, as well as provide secure performance [18], [19]. Passive RIS array gain is typically observed only when the direct communication link is severely

¹Sometimes referred to as Intelligent Reflecting Surfaces (IRS) as well. However, IRS highlights the reflecting capabilities only and the surfaces are usually not active. On the other hand, RIS highlights the reconfigurability aspect meaning that the surfaces could be passive or active and could include more functionalities as well, e.g., transmission, amplification etc. Hence, we adopt the RIS terminology in this work [13], [14], [15], [16].

0018-9545 © 2022 IEEE. Personal use is permitted, but republication/redistribution requires IEEE permission. See https://www.ieee.org/publications/rights/index.html for more information.

faded or completely blocked. Otherwise, a negligible gain is observed [20]. Moreover, the "multiplicative pathloss" or "double fading effect," of the transmitter-RIS and RIS-receiver links is usually larger than that of the direct link, which could limit the gain provided by passive RIS [21]. As a result, RIS equipped with active elements were introduced to overcome these problems through amplification of the reflected signals [17].

RIS can enhance ISAC systems as they could improve the radar component performance while extending the coverage and providing more security for the communication component of ISAC. Many works in the literature have started investigating different scenarios along these lines. For example, an efficient ISAC algorithm has been developed in [22], where a multi-layer factor graph is exploited to improve sensing performance in a multiuser multi-base station scenario. Also, in [23], joint sensing and communication has been considered for an RIS-assisted multiuser network. In this context, a graph-based approach is proposed to detect users' information and environment objects via utilizing part of the users' signals that are scattered by these objects and reflected through the RIS before arriving at the access point. In addition, RIS-assisted ISAC has been considered for a multiuser multi-target scenario in [24] to jointly maximize the users' rates and to achieve a specific design for the radar beampattern. Target detection improvement using RIS-ISAC was also addressed in [6], [25]. Also, RIS were exploited to detect non-line of sight (NLOS) multiple targets while extending the coverage of communication devices in ISAC in [26]. Furthermore, the authors of [27] discussed RIS-assisted ISAC for multiple-target sensing and multi-user communication with the existence of multiple clutters where the radar output signal-to-interference-plus-noise ratio (SINR) was maximized while maintaining the communication quality of services (QoS). Similarly, the radar receive filter, transmit beamformers and RIS phase shifts were jointly optimized in [28] to maximize the sum rate of communication users subject to a minimum received radar SNR.

A hybrid configuration of RIS containing both passive and active elements is integrated with an ISAC system in [29] in order to maximize the minimum illumination power received from a target group while considering the SINR requirements of the communication devices and the thermal noise of the active RIS elements. Finally, RIS-assisted joint radar and covert communication has been investigated in [30], and a baseline model for maximizing user's covert rates subject to a minimum radar detection probability and radar range was introduced.

B. Motivation

Along with enabling spectrum coexistence and coverage extension, and like any other communication system, RIS-ISAC systems are susceptible to threats from malicious eavesdroppers (e.g., unauthorized UAVs) [31], [32]. In fact, a few interesting challenges and game theory-based results for passive RIS-ASAC secrecy systems were recently presented in [30]. However, there is a need for designing active RIS-assisted ISAC secrecy systems with potentially high coverage gains and rigorous

radar-communication coexistence conditions, and this is the *motivation* of this paper.

In this paper, we aim to design an active RIS-ISAC secrecy system, where a multiple-antenna base station (BS) is aided by an active RIS to serve multiple users in a private region, while a malicious UAV is trying to intercept the users' data. Towards achieving this goal, we start with formulating a secrecy rate maximization problem, in which the dual radar-communication beamformers (DRC-BF), radar receive beamformers and the reflection coefficients matrix of the active RIS are jointly designed. This is subject to constraints on the worst-case signal-to-noise ratio (SNR) of the received radar signal, an upper bound on the amplification provided by the active RIS, and a maximum total transmission power budget at both the ISAC-BS and the RIS.

To this end, the problem is divided into three sub-problems. In the first one, we find a closed-form expression for the radar receive beamformers. While in the second sub-problem, the dual-functional transmit beamformers are optimized under the constraints of link power budget and radar SNR constraints. In the third sub-problem, the reflection coefficients matrix of the active RIS are designed while restricting the amplification gain and the thermal noise power of the active elements to their corresponding thresholds, along with a minimum radar SNR constraint. Finally, an efficient iterative optimization approach based on fractional programming (FP) and majorizationminimization (MM) is developed to combine the solutions of the aforementioned sub-problems. Simulation results show that the secrecy performance of the proposed active RIS-ISAC system outperforms that of the passive RIS-ISAC one and a baseline scheme where RIS are not used.

The main contributions of this article can thus be summarized as follows:

- Optimizing dual radar-communication beamformers, radar receive beamformers and reflection coefficients matrix of active RIS to maximize the secrecy rate, while guaranteeing the reliability of the radar system, and
- Introducing an iterative optimization framework that achieves convergence while combining the optimal solutions of three optimization sub-problems.

C. Paper Organization and Notation

The remaining part of this paper is organized as follows: The system and signaling models are introduced in Section II. The secrecy rate maximization problem of active RIS-assisted ISAC system is formulated in Section III while considering the radar and communication components constraints. Numerical and simulation results are then presented and discussed in Section IV before the paper is finally concluded in Section V.

Lowercase boldface letters are used for vector notations, while the uppercase boldface ones are utilized for matrices. Normal face letters are used for scalars. Mathematical fonts, e.g., \mathcal{B} are dedicated for set notation. $\mathbb{C}^{m\times n}$, $\operatorname{diag}(.)$ and $\mathbb{E}\{.\}$ denote the complex space with dimension $m\times n$, the square diagonal matrix with the elements of the input vector on its main diagonal, and the excepted value, respectively. The notation \otimes refers to the Kronecker product. $\Re\{\cdot\}$ and $\Im\{\cdot\}$ refer to the real and

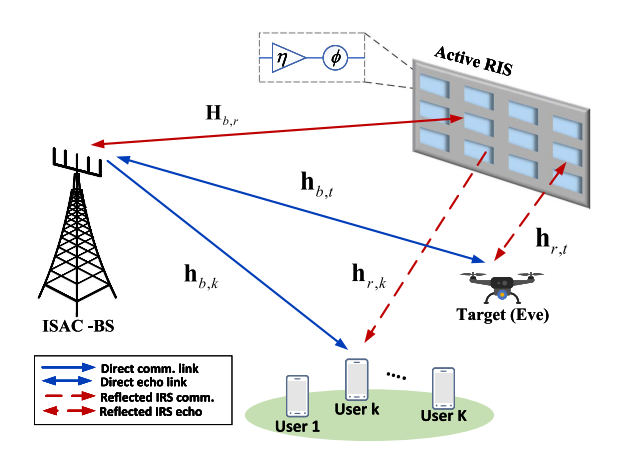


Fig. 1. Active-RIS enabled ISAC system with a malicious UAV.

imaginary parts of, respectively. Finally, \mathbf{I}_M denotes the $M \times M$ unit matrix.

II. SYSTEM MODEL

We consider an ISAC system that is assisted by an active RIS as shown in Fig. 1. In this scenario, a set of communication users $\mathcal{K} = \{1, 2, \dots, K\}$ reside in a safe private region, indicated by the green area in the figure, while a malicious UAV is hovering nearby to intercept their data. The ISAC-BS enables its radar functionality for detecting the UAV² and hence, utilizes both the transmit beamformers and active RIS capabilities to hinder the UAV operation. Each communication device and UAV is equipped with a single antenna, while the BS has M_t and M_r transmitting and receiving antennas. For the sake of simplicity, we set $M_t = M_r = M$. The active RIS is formed by stacking N active elements whose reflection coefficients form the diagonal of the matrix $\mathbf{\Phi} \in \mathbb{C}^{N \times N}$. The magnitude of the reflection coefficient of the ith element represents the amplification factor for the impinging radio wave where $|\Phi(i, i)| \leq \eta_i$ and $\eta_i > 1$ expresses the upper bound of the amplification factor of the ith element. Moreover, each element introduces a certain phase shift $arg(\Phi(i,i))$ for each incident signal as is the case in passive RIS [17]. Since we assume that the malicious UAV is hovering around the users to wiretap their channels, the Doppler frequency is set to zero.

It is worth mentioning that the active RIS-enabled system considered herein is significantly different from a traditional relay-based one, such as that using an amplify-and-forward (AF) relay, for example. Firstly, an AF relay relies on radio frequency (RF) chains, which are used for baseband signal processing. Secondly, RIS reflect the incident signals by optimizing/controlling their phase shifts, such that the reflected and direct signals could be added constructively at the receiver. Besides optimizing the phase shifts, the active RIS elements are implemented with additional power amplifiers to boost the amplitude of the reflected

signals, without further baseband processing. Accordingly, the signal model of the proposed RIS is different from that in relay-based systems. Additional differences between relays and active RIS have been extensively discussed in [17], [33], [34], [35].

A. Transmitted Signal

We assume that the ISAC-BS transmits a dual signal $\mathbf{x}[l] \in \mathbb{C}^{M \times 1}$ in each time slot l given by

$$\mathbf{x}[l] = \mathbf{W}_c \mathbf{s}_c[l] + \mathbf{W}_r \mathbf{s}_r[l] = \mathbf{W} \mathbf{s}[l], \qquad (1)$$

where $\mathbf{s}_c \in \mathbb{C}^{K \times 1}$ and $\mathbf{s}_r \in \mathbb{C}^{M \times 1}$ represent the communication symbols and radar signal, respectively, which are simultaneously transmitted with their corresponding beamformers $\mathbf{W}_c \in \mathbb{C}^{M \times K}$ and $\mathbf{W}_r \in \mathbb{C}^{M \times M}$. The radar signal is assumed to be independent of the communication symbols to avoid radar-communication mutual interference, i.e., $\mathbb{E}\{\mathbf{s}_c[l]\mathbf{s}_r^H[l]\} = \mathbf{0}$. We also assume unit powers for the communication and radar signals such that $\mathbb{E}\{\mathbf{s}_c[l]\mathbf{s}_c^H[l]\} = \mathbf{I}_K$ and $\mathbb{E}\{\mathbf{s}_r[l]\mathbf{s}_r^H[l]\} = \mathbf{I}_M$, respectively. In addition, in (1), \mathbf{W} is the DRC-BF given by $\mathbf{W} \triangleq [\mathbf{W}_c, \mathbf{W}_r] \in \mathbb{C}^{M \times (K+M)}$ and $\mathbf{s}[l] = [\mathbf{s}_c^T[l], \mathbf{s}_r^T[l]]^T \in \mathbb{C}^{(K+M) \times 1}$.

B. Radar Received Signal

According to Fig. 1, we first observe that the radar composite channel from the BS to the UAV target is given by $\mathbf{h}_{br,u}(\mathbf{\Phi}) = \mathbf{h}_{b,t}^H + \mathbf{h}_{r,t}^H \mathbf{\Phi} \mathbf{H}_{b,r} \in \mathbb{C}^{1 \times M}$, where $\mathbf{h}_{b,t} =$ $\beta_{b,t}\mathbf{a}(\theta_{b,t}) \in \mathbb{C}^{M \times 1}$, $\mathbf{h}_{r,t} = \beta_{r,t}\mathbf{a}(\theta_{r,t}) \in \mathbb{C}^{N \times 1}$ and $\mathbf{H}_{b,r} = \beta_{r,t}\mathbf{a}(\theta_{r,t})$ $\sqrt{\frac{\kappa}{\kappa+1}}\mathbf{G}_{\mathrm{LOS}} + \sqrt{\frac{1}{\kappa+1}}\mathbf{G}_{\mathrm{NLOS}} \in \mathbb{C}^{N \times M}$ represent the direct BStarget, RIS-target and BS-RIS channels, respectively. $\beta_{b,t}, \beta_{r,t}$ and κ denote the pathloss for the BS-target, RIS-target and Rician factor of the BS-RIS channels, respectively. Generally, the pathloss is defined as $\beta_{xy} = \sqrt{\delta (d_o/d_{xy})^{\bar{\alpha}_{xy}}}$, where δ is the pathloss at reference distance d_o and d_{xy} and $\bar{\alpha}_{xy}$ denote the distance between two network entities and the pathloss exponent, respectively. Finally, the LOS component of the Rician channel is expressed as $G_{LOS} = \mathbf{a}(\theta_{rb})\mathbf{a}^H(\theta_{br})$, while the NLOS component is assumed as a circular symmetric complex Gaussian random variable with zero mean. In the above, $\mathbf{a}(\theta) = \begin{bmatrix} 1, e^{-j\pi\Delta\sin(\theta)}, \dots, e^{-j\pi\Delta(M_b-1)\sin(\theta)} \end{bmatrix}^{\mathrm{T}}$ is the array response/steering vector for angle-of-arrival (AoA)/angle-ofdeparture (AoD) θ with normalized inter-element distance (w.r.t. wavelength) Δ .

Based on this, the radar echo signal, $\mathbf{y}_r[l] \in \mathbb{C}^{M \times 1}$, collected at the BS receiver from the UAV can be written as in (2) on the bottom of the next page. In (2), $\mathbf{e} \sim \mathcal{CN}(0, \sigma_e^2 \mathbf{I}_N) \in \mathbb{C}^{N \times 1}$ represents the thermal noise generated from the RIS active amplifiers elements and α is the complex-valued amplitude of the radar cross-section, where $\mathbb{E}[|\alpha|^2] = \varsigma^2$.

The first term in (2b) refers to the signal going back and forth through the direct link while the RIS-assisted echo in the second term includes the radar signal arriving through the direct link then reflecting back through the RIS, the radar signal forwarded by the RIS then reflected back through the direct path to the

²It is assumed that the target direction is typically known via defining its hovering region centered in a predefined location. Hence, optimizing the transmit and receive beamformers along with reflection coefficients matrix of the active RIS elements can be interpreted as tracking the movement of the target by predicting its location based on previous estimates [31].

BS, and the radar signal going back and forth through the RIS. Since active RIS generates thermal noise due to its amplifiers as mentioned before, this generated noise will be reflected back to the BS through two possible paths; one via the direct link and the other through the RIS. This is shown in the third and fourth terms in (2b), respectively. The fifth term represents the additional generated noise due to the reflection of $\mathbf{e}[l]$ through the RIS. The final term in (2b), $\mathbf{z}_r[l] \sim \mathcal{CN}(0, \sigma_r^2\mathbf{I}_M)$, represents the additive white Gaussian noise (AWGN) at the BS receiver with zero mean and noise power of σ_r^2 for each of the transmitting M antennas.

For simplicity, we assume that the received echo signal is much stronger than the thermal noise reflection at the radar receiver, i.e., $\|\mathbf{W}\|^2 >> \sigma_e^2$. Therefore, the received echo in (2) is simplified to

$$\mathbf{y}_{r}[l] = \alpha \mathbf{h}_{br,u}^{H}(\mathbf{\Phi}) \mathbf{h}_{br,u}(\mathbf{\Phi}) \mathbf{W} \mathbf{s}[l] + \mathbf{z}_{r}[l]. \tag{3}$$

Since Φ is diagonal, we can rewrite $\mathbf{h}_{xy}^H \Phi = \phi^{\mathrm{T}} \mathrm{diag}(\mathbf{h}_{xy}^H)$ where $\phi^{\mathrm{T}} \in \mathbb{C}^{1 \times N}$ represents the N-dimensional vector of active RIS reflection coefficients extracted from the diagonal elements of Φ . Hence, the round-trip echo channel in (3) can be written as

$$\mathbf{h}_{br,u}^{H}\left(\mathbf{\Phi}\right)\mathbf{h}_{br,u}\left(\mathbf{\Phi}\right) = \mathbf{A} + \mathbf{h}_{b,t}\boldsymbol{\phi}^{\mathrm{T}}\mathbf{B} + \mathbf{B}^{H}\boldsymbol{\phi}\mathbf{h}_{b,t}^{H} + \mathbf{B}^{H}\boldsymbol{\phi}\boldsymbol{\phi}^{\mathrm{T}}\mathbf{B}$$
$$= \mathbf{H}\left(\boldsymbol{\phi}\right). \tag{4}$$

where $\mathbf{H}(\boldsymbol{\phi}) \in \mathbb{C}^{M \times M}$, $\mathbf{A} = \mathbf{h}_{b,t} \mathbf{h}_{b,t}^H \in \mathbb{C}^{M \times M}$ and $\mathbf{B} = \operatorname{diag}(\mathbf{h}_{r,t}^H) \mathbf{H}_{b,r} \in \mathbb{C}^{N \times M}$.

By employing matched filtering, the received L samples of the echo can be expressed by $\mathbf{Y}_r \in \mathbb{C}^{M \times (K+M)}$ as

$$\mathbf{Y}_r = \alpha \mathbf{H} \left(\boldsymbol{\phi} \right) \mathbf{W} \mathbf{S} \mathbf{S}^H + \mathbf{Z} \mathbf{S}^H, \tag{5}$$

where $\mathbf{Z} = [\mathbf{z}_r[1], \dots, \mathbf{z}_r[L]] \in \mathbb{C}^{M \times L}$, and $\mathbf{S} = [\mathbf{s}[1], \dots, \mathbf{s}[L]] \in \mathbb{C}^{(K+M) \times L}$. Equation (5) can be vectorized by defining the following: $\tilde{\mathbf{y}}_r \triangleq \text{vec}\{\mathbf{Y}_r\} \in \mathbb{C}^{M(K+M) \times 1}$, $\tilde{\mathbf{z}}_r \triangleq \text{vec}\{\mathbf{Z}\mathbf{S}^H\} \in \mathbb{C}^{M(K+M) \times 1}$ and $\tilde{\mathbf{w}} \triangleq \text{vec}\{\mathbf{W}\} \in \mathbb{C}^{M(K+M) \times 1}$. Hence, we have

$$\tilde{\mathbf{y}}_r = \alpha \left(\mathbf{S} \mathbf{S}^H \otimes \mathbf{H} \left(\boldsymbol{\phi} \right) \right) \tilde{\mathbf{w}} + \tilde{\mathbf{z}}_r. \tag{6}$$

The received echo is post-processed by the receive beamformers, $\mathbf{u} \in \mathbb{C}^{M(K+M) \times 1}$, which yields

$$\mathbf{u}^{H}\tilde{\mathbf{y}}_{r} = \alpha \mathbf{u}^{H} \left(\mathbf{S}\mathbf{S}^{H} \otimes \mathbf{H} \left(\boldsymbol{\phi} \right) \right) \tilde{\mathbf{w}} + \mathbf{u}^{H} \text{vec} \left\{ \mathbf{Z}\mathbf{S}^{H} \right\}.$$
 (7)

Accordingly, the radar output SNR can be expressed as

$$SNR_{r} = \frac{\varsigma^{2} \mathbb{E}_{S} \left\{ \left| \mathbf{u}^{H} \left(\mathbf{S} \mathbf{S}^{H} \otimes \mathbf{H} \left(\boldsymbol{\phi} \right) \right) \tilde{\mathbf{w}} \right|^{2} \right\}}{\sigma_{r}^{2} \mathbf{u}^{H} \mathbf{u}}.$$
 (8)

It is worth mentioning here that the active RIS thermal noise reflection has been neglected in (8). The reason behind that has to do with the fact that had the active RIS thermal noise reflection been considered, the denominator of the radar output SNR would include terms involving the round-trip multiplicative channel losses (i.e., path losses and instantaneous channels), which have insignificant contribution.

The received echo SNR can be approximated using Jensen's inequality $\mathbb{E}\{f(x)\} \geq f(\mathbb{E}\{x\})$ where the numerator can be lower bounded as

$$\mathbb{E}_{\mathbf{S}}\left\{\left|\mathbf{u}^{H}\left(\mathbf{S}\mathbf{S}^{H}\otimes\mathbf{H}\left(\boldsymbol{\phi}\right)\right)\tilde{\mathbf{w}}\right|^{2}\right\}\geq L\left|\mathbf{u}^{H}\left(\mathbf{I}_{K+M}\otimes\mathbf{H}\left(\boldsymbol{\phi}\right)\right)\tilde{\mathbf{w}}\right|^{2}$$

$$=L\left|\mathbf{u}^{H}\tilde{\mathbf{H}}\left(\boldsymbol{\phi}\right)\tilde{\mathbf{w}}\right|^{2},\tag{9}$$

where $\mathbb{E}_{\mathbf{S}}\{\mathbf{S}\mathbf{S}^H\} = L\mathbf{I}_{K+M}$ and $\tilde{\mathbf{H}}(\phi) = \mathbf{I}_{K+M} \otimes \mathbf{H}(\phi)$. By substituting (9) into (8), we can obtain the worst-case SNR of the received echo signal at the radar output as

$$SNR_r \ge \frac{L\varsigma^2 \left| \mathbf{u}^H \tilde{\mathbf{H}} \left(\boldsymbol{\phi} \right) \tilde{\mathbf{w}} \right|^2}{\sigma_r^2 \mathbf{u}^H \mathbf{u}}.$$
 (10)

C. Communications Received Signal

The received signal at the legitimate communication user $k \in \mathcal{K}$ in the lth time slot can be expressed as

$$y_k[l] = \mathbf{h}_{br,k}(\mathbf{\Phi}) \mathbf{x}[l] + \mathbf{h}_{r,k}^H \mathbf{\Phi} \mathbf{e}[l] + z_k[l], \quad (11)$$

where $\mathbf{h}_{br,k}(\mathbf{\Phi}) = \mathbf{h}_{b,k}^H + \mathbf{h}_{r,k}^H \mathbf{\Phi} \mathbf{H}_{b,r} \in \mathbb{C}^{1 \times M}$ is the composite communication channel from the BS to user k and $z_k[l] \sim \mathcal{CN}(0,\sigma_k^2)$ represents the AWGN at its receiver. The first term in (11) represents the desired communication signal, whereas the second one is the added active RIS noise. Similarly, the received information signal at the malicious UAV is given by

$$y_u[l] = \mathbf{h}_{br,u}(\mathbf{\Phi}) \mathbf{x}[l] + \mathbf{h}_{r,t}^H \mathbf{\Phi} \mathbf{e}[l] + z_u[l], \qquad (12)$$

where $\mathbf{h}_{br,u}(\mathbf{\Phi}) = \mathbf{h}_{b,t}^H + \mathbf{h}_{r,t}^H \mathbf{\Phi} \mathbf{H}_{b,r} \in \mathbb{C}^{1 \times M}$ is the composite communication channel from the BS to the UAV and $z_u[l] \sim \mathcal{CN}(0,\sigma_u^2)$ is the AWGN at its receiver. For the sake of simplicity, we assume equal noise variances for all communication and radar equipment and we set it to σ^2 , i.e., $\sigma_k^2 = \sigma_u^2 = \sigma_r^2 = \sigma^2$.

The received SINR at the kth user is thus obtained as

$$SINR_{k} = \frac{\|\mathbf{h}_{br,k}(\boldsymbol{\Phi})\mathbf{w}_{k}\|^{2}}{\sum_{j=1,j\neq k}^{K+M} \|\mathbf{h}_{br,k}(\boldsymbol{\Phi})\mathbf{w}_{j}\|^{2} + \sigma_{e}^{2} \|\mathbf{h}_{r,k}^{H}\boldsymbol{\Phi}\|^{2} + \sigma^{2}}$$

$$= \frac{\mathbf{h}_{br,k}(\boldsymbol{\Phi})\bar{\mathbf{W}}_{k}\mathbf{h}_{br,k}^{H}(\boldsymbol{\Phi})}{\mathbf{h}_{br,k}(\boldsymbol{\Phi})\left(\sum_{j=1,j\neq k}^{K+M} \bar{\mathbf{W}}_{j}\right)\mathbf{h}_{br,k}^{H}(\boldsymbol{\Phi}) + \sigma_{e}^{2} \|\mathbf{h}_{r,k}^{H}\boldsymbol{\Phi}\|^{2} + \sigma^{2}}, \tag{13}$$

$$\mathbf{y}_{r}\left[l\right] = \alpha(\mathbf{h}_{b,t} + \mathbf{H}_{br}^{H} \mathbf{\Phi}^{H} \mathbf{h}_{r,t}) \left[(\mathbf{h}_{b,t}^{H} + \mathbf{h}_{r,t}^{H} \mathbf{\Phi} \mathbf{H}_{b,r}) \mathbf{x}\left[l\right] + \mathbf{h}_{r,t}^{H} \mathbf{\Phi} \mathbf{e}\left[l\right] \right] + \mathbf{H}_{br}^{H} \mathbf{\Phi}^{H} \mathbf{e}_{o}\left[l\right] + \mathbf{z}_{r}\left[l\right]$$

$$= \underbrace{\alpha \mathbf{h}_{b,t} \mathbf{h}_{b,t}^{H} \mathbf{W} \mathbf{s}\left[l\right]}_{\text{Echo of direct link}} + \underbrace{\alpha \left(\mathbf{h}_{b,t} \mathbf{h}_{r,t}^{H} \mathbf{\Phi} \mathbf{H}_{b,r} + \mathbf{H}_{br}^{H} \mathbf{\Phi}^{H} \mathbf{h}_{r,t} \mathbf{h}_{b,t}^{H} + \mathbf{H}_{br}^{H} \mathbf{\Phi}^{H} \mathbf{h}_{r,t} \mathbf{h}_{r,t}^{H} \mathbf{\Phi} \mathbf{H}_{b,r}\right) \mathbf{W} \mathbf{s}\left[l\right]}_{\text{RIS noise direct to BS}} + \underbrace{\alpha \mathbf{H}_{br}^{H} \mathbf{\Phi}^{H} \mathbf{h}_{r,t} \mathbf{h}_{r,t}^{H} \mathbf{\Phi} \mathbf{e}\left[l\right]}_{\text{RIS noise reflection through RIS}} + \underbrace{\mathbf{H}_{br}^{H} \mathbf{\Phi}^{H} \mathbf{e}_{o}\left[l\right]}_{\text{Added noise in reflection of } \mathbf{e}\left[l\right]}_{\text{Added noise in reflection of } \mathbf{e}\left[l\right]}$$

$$(2b)$$

where $\mathbf{w}_j \in \mathbb{C}^{M \times 1}$ represents the *j*th column of \mathbf{W} and $\bar{\mathbf{W}}_j = \mathbf{w}_j \mathbf{w}_j^H \in \mathbb{C}^{M \times M}$. The first term of the denominator represents multi-user interference, while the second and third terms represent both the active RIS thermal noise and AWGN effects. Similarly, the received SINR at the malicious UAV is given by

$$SINR_{u} = \frac{\sum_{i=1}^{K+M} \|\mathbf{h}_{br,u}\left(\mathbf{\Phi}\right)\mathbf{w}_{i}\|^{2}}{\sigma_{e}^{2} \|\mathbf{h}_{r,t}^{H}\mathbf{\Phi}\|^{2} + \sigma^{2}}$$

$$= \frac{\mathbf{h}_{br,u}\left(\mathbf{\Phi}\right)\left(\sum_{i=1}^{K+M} \bar{\mathbf{W}}_{i}\right)\mathbf{h}_{br,u}^{H}\left(\mathbf{\Phi}\right)}{\sigma_{e}^{2} \|\mathbf{h}_{r,t}^{H}\mathbf{\Phi}\|^{2} + \sigma^{2}}.$$
(14)

From (13) and (14), the achievable sum data rate at the legitimate users and the UAV are given by $R_c = \sum_{k=1}^K R_k = \sum_{k=1}^K \log_2(1+\mathrm{SINR}_k)$ and $R_u = \log_2(1+\mathrm{SINR}_u)$, respectively. It is assumed that the BS has perfect estimates of the users' channel state information (CSI) via one of the channel estimation techniques and also knows the CSI of the UAV via efficient sensing [32]. Based on the above, the secrecy rate of the system can be written as $R_c - R_u$.

III. PROBLEM FORMULATION AND PROPOSED OPTIMIZATION FRAMEWORK

In this section, we consider a constrained secrecy rate maximization problem via jointly designing the transmit W and receive u beamformers as well as the reflection matrix Φ of the active RIS elements. The optimization problem is formulated as

subject to:

$$SNR_r \approx \frac{L\varsigma^2 \left| \mathbf{u}^H \tilde{\mathbf{H}} \left(\boldsymbol{\phi} \right) \tilde{\mathbf{w}} \right|^2}{\sigma^2 \mathbf{u}^H \mathbf{u}} \ge \gamma_t, \tag{15b}$$

$$\|\mathbf{W}\|_F^2 \le P_o,\tag{15c}$$

$$\|\mathbf{\Phi}\mathbf{H}_{b,r}\mathbf{w}_i\|^2 + \sigma_e^2 \|\mathbf{\Phi}\|^2 \le \bar{P}_I,$$

$$\forall i \in \{1, \dots, K + M\}, \tag{15d}$$

$$|\mathbf{\Phi}(n,n)| \le \eta_n, \forall n \in \{1,\dots,N\},\,$$
 (15e)

The first constraint (15b) ensures proper target detection performance via guaranteeing a minimum radar SNR γ_t . The total transmission power budget is enforced by constraints (15c) and (15d) where P_0 is the maximum allowed transmission power at the BS with $\|.\|_F$ representing the Frobenius Norm while the power generated by the active RIS elements is restricted to $\bar{P}_I = \frac{P_I}{K+M}$ for each of the virtual K+M downlink streams. Moreover, the magnitude of the active RIS elements reflection coefficients is upper bounded by $\eta_n \ge 1$ as in constraint (15e). Therefore, the total power of the active RIS-assisted ISAC is divided into two parts: the first is at the BS while the other is consumed in the active RIS elements. Comparing with the passive RIS-assisted schemes, power is only consumed at the BS and for fair comparison, as will be shown later, this should be equal to the sum of the former two parts of the active RIS-based scenario.

It is worth mentioning here that the RIS amplification power is modelled based on the classical power amplifier model in [36]. In this model, the amplification power of the reflecting elements depends on the DC biasing power (consumed at each element), the control circuit power, the RIS amplifiers' efficiency and the output/reflected power, which includes the thermal noise power. Accordingly, the power budget of the active RIS subsumes the thermal noise power as demonstrated in [34, Eqs. (10)–(14)]. Specifically, the active RIS power budget is given by $\bar{P}_I = \frac{1}{K+M}(N(P_c+P_{DC})+\eta(p_t\|\Phi\mathbf{H}_{b,r}\|^2+\sigma_e^2\|\Phi\|^2))$, where P_c, P_{DC} and η denote the control circuit power, the DC biasing power and the RIS amplifier efficiency, respectively.

The problem in (15) is non-convex. In order to solve it, we divide it into three sub-problems; each trying to optimize one of the three variables W, u, Φ in an iterative manner using MM and FP techniques as will be detailed in the sequel.

A. Optimizing the Radar Receive Beamformers u

Given the DRC-BF and the RIS reflection coefficients matrix W, Φ , the receive beamforming problem is reduced to the well-known "Rayleigh quotient" optimization problem [27], given by

Maximize
$$\left|\mathbf{u}^{H}\tilde{\mathbf{H}}\left(\boldsymbol{\phi}\right)\tilde{\mathbf{w}}\right|^{2}$$
 subject to $\left\|\mathbf{u}\right\|^{2}=1,$ (16)

which is solved in closed form as $\mathbf{u}_{\mathrm{opt}} = \frac{\tilde{\mathbf{H}}(\phi)\tilde{\mathbf{w}}}{\tilde{\mathbf{w}}^H\overline{\mathbf{H}}(\phi)\tilde{\mathbf{w}}}$, where $\overline{\mathbf{H}}(\phi) = \mathbf{I}_{K+M} \otimes \mathbf{H}^H(\phi)\mathbf{H}(\phi)$. Moreover, we note that an arbitrary change in the phase of $\mathbf{u}^H\tilde{\mathbf{y}}_r$ does not affect the received radar SNR in (8). Hence, we can consider $\mathbf{u}_{\mathrm{opt}}e^{j\theta}$ as an optimal receive beamformer for (16) for any arbitrary target angle θ .

B. Optimizing the DRC-BF W

Given the receive beamformers u and the reflection coefficients matrix of the active RIS, Φ , the DRC-BF optimization problem is expressed as

$$\operatorname{Maximize}_{\mathbf{W}} R_c - R_u \tag{17a}$$

subject to:

$$\frac{L\varsigma^{2}\left|\mathbf{u}^{H}\tilde{\mathbf{H}}\left(\boldsymbol{\phi}\right)\tilde{\mathbf{w}}\right|^{2}}{\sigma^{2}\mathbf{u}^{H}\mathbf{u}} \geq \gamma_{t},$$
(17b)

$$\|\mathbf{W}\|_F^2 \le P_o,\tag{17c}$$

$$\|\mathbf{\Phi}\mathbf{H}_{b,r}\mathbf{w}_{i}\|^{2} + \sigma_{e}^{2}\|\mathbf{\Phi}\|^{2} \leq \bar{P}_{I},$$

$$\forall i \in \{1, \dots, K + M\}, \qquad (17d)$$

which is a non-convex problem due to the non-concave objective since it is a difference between two log functions. Hereafter, we rewrite the objective in a convex form with respect to the optimization variable \boldsymbol{W} as given by the following Lemma.

Lemma 1: By resorting to the FP approach in [37], the objective in (17) could be simply expressed as

$$R_c - R_u = \varepsilon + \Re \left\{ \mathbf{a}^H \tilde{\mathbf{w}} \right\} - \left\| \ddot{\mathbf{B}} \tilde{\mathbf{w}} \right\|^2, \tag{18}$$

where $\ddot{\mathbf{B}}$, ε and \mathbf{a} are given by (42), (50) and (51), respectively. *Proof:* See Appendix A.

Now, with the optimal receive beamformers in the previous subsection, the numerator of constraint (17b) could be restricted to real and non-negative values as

$$\Re\left\{\mathbf{u}^{H}\tilde{\mathbf{H}}\left(\boldsymbol{\phi}\right)\tilde{\mathbf{w}}\right\} \geq \sqrt{\frac{\sigma^{2}\gamma_{t}\mathbf{u}^{H}\mathbf{u}}{L\varsigma^{2}}},$$
(19)

which is convex. Constraints (17c) and (17d) can also be recast in convex forms as

$$\operatorname{tr}\left\{\mathbf{W}\mathbf{W}^{H}\right\} \leq P_{o},\tag{20}$$

$$\operatorname{tr}\left\{\mathbf{\Phi}\mathbf{H}_{b,r}\mathbf{w}_{i}\mathbf{w}_{i}^{H}\mathbf{H}_{br}^{H}\mathbf{\Phi}^{H}\right\} \leq \tilde{P}_{I},\tag{21}$$

where $\tilde{P}_I = \bar{P}_I - \sigma_e^2 \|\Phi\|^2$. Substituting (18)–(21) into (17) yields the following dual-functional beamforming optimization problem:

Maximize
$$\Re\left\{\mathbf{a}^{H}\tilde{\mathbf{w}}\right\} - \left\|\ddot{\mathbf{B}}\tilde{\mathbf{w}}\right\|^{2}$$
 (22a)

subject to:

$$\Re\left\{\mathbf{u}^{H}\tilde{\mathbf{H}}\left(\boldsymbol{\phi}\right)\tilde{\mathbf{w}}\right\} \geq \sqrt{\frac{\sigma^{2}\gamma_{t}\mathbf{u}^{H}\mathbf{u}}{L\varepsilon^{2}}},$$
 (22b)

$$\operatorname{tr}\left\{\mathbf{W}\mathbf{W}^{H}\right\} \leq P_{o},\tag{22c}$$

$$\operatorname{tr}\left\{\mathbf{\Phi}\mathbf{H}_{b,r}\bar{\mathbf{W}}_{i}\mathbf{H}_{br}^{H}\mathbf{\Phi}^{H}\right\} \leq \tilde{P}_{I},\tag{22d}$$

Now, problem (22) is convex and can be solved using standard convex optimization tools such as the CVX solver [38].

C. Optimizing the Reflection Coefficients Matrix Φ

With fixed variables W and u, the reflection coefficients matrix of the active RIS can be optimized through

$$Maximize R_c - R_u$$
 (23a)

subject to:

$$\Re\left\{\mathbf{u}^{H}\tilde{\mathbf{H}}\left(\boldsymbol{\phi}\right)\tilde{\mathbf{w}}\right\} \geq \sqrt{\frac{\sigma^{2}\gamma_{t}\mathbf{u}^{H}\mathbf{u}}{L\varsigma^{2}}},$$
 (23b)

$$|\mathbf{\Phi}(n,n)| \le \eta_n, \forall n \in \{1,\ldots,N\},$$
 (23c)

$$\|\mathbf{\Phi}\mathbf{H}_{b,r}\mathbf{w}_i\|^2 + \sigma_e^2 \|\mathbf{\Phi}\|^2 \le \bar{P}_I,$$
 (23d)

which is a non-convex problem due to the non-concave objective and constraint (23b). We start with the objective function and introduce the following corollary in which the objective function is expressed in a compact form as an explicit function of the active RIS reflection coefficients matrix. We will then use this result to help us express the objective function in convex form with respect to ϕ as will be shown in the sequel.

Corollary 1: According to the result of Lemma 1, the objective in (23a) can be represented explicitly as a function of the active RIS reflection coefficients matrix ϕ as

$$R_c - R_u = \bar{\varepsilon} + \Re \left\{ \mathbf{v}^H \boldsymbol{\phi} \right\} - \boldsymbol{\phi}^H \mathbf{Q} \boldsymbol{\phi} \tag{24}$$

where \mathbf{v} , \mathbf{Q} and $\bar{\varepsilon}$ are given by (56), (57) and (58), respectively. *Proof:* See Appendix B.

In order to proceed with (23b), we have to extract the variable Φ out of the Kronecker expression inside $\tilde{\mathbf{H}}(\phi)$ through the following manipulations. We first reformulate the product $\tilde{\mathbf{H}}(\phi)\tilde{\mathbf{w}}$ as follows:

$$\tilde{\mathbf{H}}(\boldsymbol{\phi})\,\tilde{\mathbf{w}} = \mathbf{I}_{K+M} \otimes \left(\mathbf{A} + \mathbf{h}_{b,t}\boldsymbol{\phi}^{\mathrm{T}}\mathbf{B} + \mathbf{B}^{H}\boldsymbol{\phi}\mathbf{h}_{b,t}^{H} + \mathbf{B}^{H}\boldsymbol{\phi}\boldsymbol{\phi}^{\mathrm{T}}\mathbf{B}\right)\tilde{\mathbf{w}}$$

$$= \left(\mathbf{I}_{K+M} \otimes \mathbf{A}\right)\tilde{\mathbf{w}} + \left(\mathbf{I}_{K+M} \otimes \mathbf{h}_{b,t}\boldsymbol{\phi}^{\mathrm{T}}\mathbf{B}\right)\tilde{\mathbf{w}}$$

$$+ \left(\mathbf{I}_{K+M} \otimes \mathbf{B}^{H}\boldsymbol{\phi}\mathbf{h}_{b,t}^{H}\right)\tilde{\mathbf{w}} + \left(\mathbf{I}_{K+M} \otimes \mathbf{B}^{H}\boldsymbol{\phi}\boldsymbol{\phi}^{\mathrm{T}}\mathbf{B}\right)\tilde{\mathbf{w}}.$$
(25)

Then, we utilize the Kronecker product property: $\text{vec}\{\mathbf{ABC}\} = (\mathbf{C}^T \otimes \mathbf{A})\text{vec}\{\mathbf{B}\}$ to write the individual terms of (25) as follows:

$$(\mathbf{I}_{K+M} \otimes \mathbf{h}_{b,t} \boldsymbol{\phi}^{\mathrm{T}} \mathbf{B}) \, \tilde{\mathbf{w}} = \operatorname{vec} \left\{ \mathbf{h}_{b,t} \boldsymbol{\phi}^{\mathrm{T}} \mathbf{B} \mathbf{W} \right\}$$

$$= \left((\mathbf{B} \mathbf{W})^{\mathrm{T}} \otimes \mathbf{h}_{b,t} \right) \boldsymbol{\phi}, \qquad (26)$$

$$(\mathbf{I}_{K+M} \otimes \mathbf{B}^{H} \boldsymbol{\phi} \mathbf{h}_{b,t}^{H}) \, \tilde{\mathbf{w}} = \operatorname{vec} \left\{ \mathbf{B}^{H} \boldsymbol{\phi} \mathbf{h}_{b,t}^{H} \mathbf{W} \mathbf{I}_{K+M} \right\}$$

$$= \left((\mathbf{h}_{b,t}^{H} \mathbf{W})^{\mathrm{T}} \otimes \mathbf{B}^{H} \right) \boldsymbol{\phi}, \qquad (27)$$

$$\left(\mathbf{I}_{K+M} \otimes \mathbf{B}^{H} \boldsymbol{\phi} \boldsymbol{\phi}^{\mathrm{T}} \mathbf{B} \right) \, \tilde{\mathbf{w}}$$

$$= \operatorname{vec} \left\{ \mathbf{B}^{H} \boldsymbol{\phi} \boldsymbol{\phi}^{\mathrm{T}} \mathbf{B} \mathbf{W} \mathbf{I}_{K+M} \right\}$$

$$= \left((\mathbf{B} \mathbf{W})^{\mathrm{T}} \otimes \mathbf{B}^{H} \right) \operatorname{vec} \left\{ \boldsymbol{\phi} \boldsymbol{\phi}^{\mathrm{T}} \right\}. \qquad (28)$$

Substituting (26)–(28) into (23b) leads to the following form for the SNR radar constraint:

$$\Re\left\{\mathbf{b}_{o}\boldsymbol{\phi} + \boldsymbol{\phi}^{\mathrm{T}}\tilde{\mathbf{C}}_{0}\boldsymbol{\phi}\right\} \geq \sqrt{\frac{\sigma^{2}\gamma_{t}\mathbf{u}^{H}\mathbf{u}}{L\varsigma^{2}}} - \Re\left\{a_{o}\right\}, \qquad (29)$$

where

$$a_o = \mathbf{u}^H \left(\mathbf{I}_{K+M} \otimes \mathbf{A} \right) \tilde{\mathbf{w}},\tag{30}$$

$$\mathbf{b}_{o} = \mathbf{u}^{H} \left[\left(\mathbf{B} \mathbf{W} \right)^{\mathrm{T}} \otimes \mathbf{h}_{b,t} + \left(\mathbf{h}_{b,t}^{H} \mathbf{W} \right)^{\mathrm{T}} \otimes \mathbf{B}^{H} \right] \in \mathbb{C}^{1 \times N}, \tag{31}$$

$$\mathbf{c}_0 = \mathbf{u}^H \left((\mathbf{B}\mathbf{W})^{\mathrm{T}} \otimes \mathbf{B}^H \right) \in \mathbb{C}^{1 \times N^2},$$
 (32)

and $\tilde{\mathbf{C}}_0 \in \mathbb{C}^{N \times N}$ is a reshaped matrix from $\mathbf{c}_o^{\mathrm{T}}$ such that $\mathbf{c}_o^{\mathrm{T}} = \text{vec}\{\tilde{\mathbf{C}}_0\}$.

Unfortunately, constraint (29) is still non-convex since the real part of $\phi^T \tilde{\mathbf{C}}_0 \phi$ is a non-concave function. Moreover, the semidefiniteness of Q, in (24), is not guaranteed. To tackle these issues, we convert this term into an alternative real form $\bar{\phi}^T \bar{\mathbf{C}}_0 \bar{\phi}$ as follows. We first define $\bar{\phi} \triangleq \left[\Re\{\phi^T\}\ \Im\{\phi^T\}\right]^T$ with

dimensions $2N \times 1$ and the $2N \times 2^{\sim}N$ matrix

$$\bar{\mathbf{C}}_0 \triangleq \begin{bmatrix} \Re \left\{ \tilde{\mathbf{C}}_0 \right\} & -\Im \left\{ \tilde{\mathbf{C}}_0 \right\} \\ -\Im \left\{ \tilde{\mathbf{C}}_0 \right\} & -\Re \left\{ \tilde{\mathbf{C}}_0 \right\} \end{bmatrix}.$$

We then apply the MM technique [39] to find the corresponding surrogate function. Particularly, with a given ϕ at specific iteration/point (t), $\phi^{(t)}$, the first order Taylor approximation of $\bar{\boldsymbol{\phi}}^{\mathrm{T}}\bar{\mathbf{C}}_{0}\bar{\boldsymbol{\phi}}$ is lower bounded as

$$\bar{\boldsymbol{\phi}}^{\mathrm{T}} \bar{\mathbf{C}}_{0} \bar{\boldsymbol{\phi}} \geq \left(\bar{\boldsymbol{\phi}}^{\mathrm{T}} \bar{\mathbf{C}}_{0} \bar{\boldsymbol{\phi}} \right)^{(t)} + \left(\bar{\boldsymbol{\phi}}^{\mathrm{T}} \right)^{(t)} \left(\bar{\mathbf{C}}_{0} + \bar{\mathbf{C}}_{o}^{\mathrm{T}} \right) \left(\bar{\boldsymbol{\phi}} - \left(\bar{\boldsymbol{\phi}} \right)^{(t)} \right)
= - \left(\bar{\boldsymbol{\phi}}^{\mathrm{T}} \bar{\mathbf{C}}_{0}^{\mathrm{T}} \bar{\boldsymbol{\phi}} \right)^{(t)} + \Re \left\{ \left(\bar{\boldsymbol{\phi}}^{\mathrm{T}} \right)^{(t)} \left(\bar{\mathbf{C}}_{0} + \bar{\mathbf{C}}_{o}^{\mathrm{T}} \right) \boldsymbol{\Pi} \boldsymbol{\phi} \right\}
= - \overline{\bar{\mathbf{C}}}_{o}^{(t)} + \Re \left\{ \tilde{\boldsymbol{\Pi}}_{o}^{(t)} \boldsymbol{\phi} \right\},$$
(33)

where $\Pi = [\mathbf{I}_N \ j \mathbf{I}_N]^{\mathrm{T}} \in \mathbb{C}^{2N \times N}, \ \overline{\overline{\mathbf{C}}}_o^{(t)} = \left(\bar{\boldsymbol{\phi}}^{\mathrm{T}} \bar{\mathbf{C}}_0^{\mathrm{T}} \bar{\boldsymbol{\phi}}\right)^{(t)}$ $\tilde{\mathbf{\Pi}}_o^{(t)} = \left(\bar{\boldsymbol{\phi}}^{\mathrm{T}}\right)^{(t)} (\bar{\mathbf{C}}_0 + \bar{\mathbf{C}}_o^{\mathrm{T}}) \mathbf{\Pi}$. By substituting (33) into (29), the SNR detection constraint can be rewritten as

$$\Re\left\{\mathbf{d}_{o}\boldsymbol{\phi}\right\} \geq \tilde{\varepsilon},\tag{34}$$

where
$$\mathbf{d}_o = \mathbf{b}_o + \tilde{\mathbf{\Pi}}_o^{(t)}$$
 and $\tilde{\varepsilon} = \sqrt{\frac{\sigma^2 \gamma_t \mathbf{u}^H \mathbf{u}}{L\varsigma^2}} - \Re\{\mathbf{u}_{opt}^H(\mathbf{I}_{K+M} \otimes \mathbf{h}_{b,t} \mathbf{h}_{b,t}^H) \tilde{\mathbf{w}}\} + \overline{\overline{\mathbf{C}}}_o^{(t)}$. Constraint (34) is now convex due to the concavity of its left-hand side.

Now, going back to the new form of the objective function in (24), it is possible to follow the same approach to re-express the $\begin{array}{l} \boldsymbol{\phi}^H \mathbf{Q} \boldsymbol{\phi} \text{ term as follows: } \boldsymbol{\phi}^H \mathbf{Q} \boldsymbol{\phi} \geq -\overline{\overline{\mathbf{Q}}}^{(t)} + \Re\{\tilde{\mathbf{\Pi}}_q^{(t)} \boldsymbol{\phi}\}, \text{ where } \\ \overline{\overline{\mathbf{Q}}}^{(t)} = \left(\overline{\boldsymbol{\phi}}^\mathrm{T} \bar{\mathbf{Q}}^\mathrm{T} \overline{\boldsymbol{\phi}}\right)^{(t)}, \ \bar{\mathbf{Q}} \triangleq \begin{bmatrix} \Re\{\mathbf{Q}\} & -\Im\{\mathbf{Q}\} \\ -\Im\{\mathbf{Q}\} & -\Re\{\mathbf{Q}\} \end{bmatrix} \text{ and } \tilde{\mathbf{\Pi}}_q^{(t)} = \end{array}$ $\left(\overline{\boldsymbol{\phi}}^{\mathrm{T}}\right)^{(t)}(\bar{\mathbf{Q}}+\bar{\mathbf{Q}}^{\mathrm{T}})\mathbf{\Pi}.$

According to previous analysis, we can recast the reflection coefficients matrix optimization problem, after dropping the constant terms, as follows:

$$\underset{\phi}{\text{Minimize }} \Re\left\{ \bar{\mathbf{v}}_{q} \phi \right\} \tag{35a}$$

subject to:

$$\Re\left\{\mathbf{d}_{o}\boldsymbol{\phi}\right\} \geq \tilde{\varepsilon},\tag{35b}$$

$$|\phi[n]| \le \eta_n, \quad \forall n \in \{1, ..., N\},$$
 (35c)

$$\boldsymbol{\phi}^{H}\left(\Lambda_{i} + \sigma_{e}^{2}\mathbf{I}\right)\boldsymbol{\phi} \leq \bar{P}_{I}, \quad \forall i \in \{1, ..., K + M\},$$
 (35d)

 $ar{\mathbf{v}}_q = ilde{\mathbf{\Pi}}_q^{(t)} - \mathbf{v}^H$ $\operatorname{diag}\{\mathbf{H}_{b,r}\mathbf{w}_i\}\operatorname{diag}\{\mathbf{H}_{b,r}\mathbf{w}_i\}^H$. As a consequence, problem (35) is now in convex form that can be handled efficiently by one of standard convex optimization tools such as the CVX solver as mentioned earlier [38].

D. Overall Optimization Framework

Algorithm 1 summarizes the proposed overall iterative approach to find the optimal values of u, W and Φ , where $x^{(t-1)}$ denotes the variable \boldsymbol{x} obtained at the (t-1)-th iteration. The

Algorithm 1: Joint optimization algorithm for active-RIS assisted secure ISAC.

- 1: Set the initial values $\boldsymbol{W}^{(0)}, \boldsymbol{u}^{(0)}, \boldsymbol{\phi}^{(0)}, c_k^{(0)}, c_u^{(0)}, \gamma_k^{(0)}, \gamma_u^{(0)}$ and iteration index t = 1
- 2: repeat
- 3: Evaluate $c_k^{(t)}$ by solving (40) given $\boldsymbol{W}^{(t-1)}, \boldsymbol{u}^{(t-1)}, \boldsymbol{\phi}^{(t-1)}, c_u^{(t-1)}, \gamma_k^{(t-1)}$ and $\gamma_u^{(t-1)}$.
- 4: Calculate $\gamma_k^{(t)}$ by solving (39) given the other variables
- at t-1. 5: Find $c_u^{(t)}$ by solving (47) given the other variables at
- 6: Update $\gamma_u^{(t)}$ by solving (46) given the other variables
- 7: Calculate $\boldsymbol{u}^{(t)} = \frac{\tilde{\mathbf{H}}(\boldsymbol{\phi})\tilde{\mathbf{w}}}{\tilde{\mathbf{w}}^H \tilde{\mathbf{H}}(\boldsymbol{\phi})\tilde{\mathbf{w}}}$ given $\boldsymbol{W}^{(t-1)}, \boldsymbol{\phi}^{(t-1)},$ $c_k^{(t-1)}, c_u^{(t-1)}, \gamma_k^{(t-1)}$ and $\gamma_u^{(t-1)}$.

 8: Update $\boldsymbol{W}^{(t)}$ via solving (22) with the other variables
- Update $\phi^{(t)}$ via solving (35) with the other variables
- Update t = t + 1.
- 11: until convergence.

first line of the algorithm sets feasible initializations for the optimization variables. In lines 2 to 9, all the optimization variables are obtained by solving their corresponding optimization problems and are updated iteratively until convergence is reached. The convergence of Algorithm 1 is guaranteed due to the non-increasing property of the auxiliary variables $\{\gamma_k, c_k, \gamma_u, c_u\}$ as well as the boundedness of both **W** and ϕ through the corresponding constraints [37]. This will be clearly seen in the simulation results section as well.

IV. SIMULATION RESULTS

In this section, we evaluate the performance of the proposed system using Monte Carlo simulations, where the secrecy performance is averaged over 500 channel realizations. We assume that both the BS and active RIS are equipped with a uniform linear array (ULA) with M=6 and N=10 antennas, respectively, with half-wave length spacing in between the elements. For simplicity, we assume an equal amplification factor for each element of the RIS, i.e., $\eta_n = \eta \ \forall n \in \{1, 2, \dots, N\}$. Without loss of generality, we consider a simulation environment with dimensions $300 \times 300 \text{ m}^2$ where the BS and the active RIS are located at [0, 0] and [250, 50] m, respectively and the number of legitimate devices is set to K = 4 randomly distributed in a circle with radius r = 50 m centered at [150, -100]. The malicious UAV is assumed to be hovering within a circle centered at [250, -50] with radius r = 50 m and fixed altitude h = 50m. Fig. 2 mimics an instance of the proposed system setup. The radar cross-section, the number of collected samples, and the radar detection threshold are set to $\zeta^2 = 1$, L = 1000, and $\gamma_r = 5 \, \mathrm{dB}$, respectively. Moreover, the noise level at all receivers is set to $\sigma^2 = -80$ dBm. The Rician coefficients for the BS-RIS,

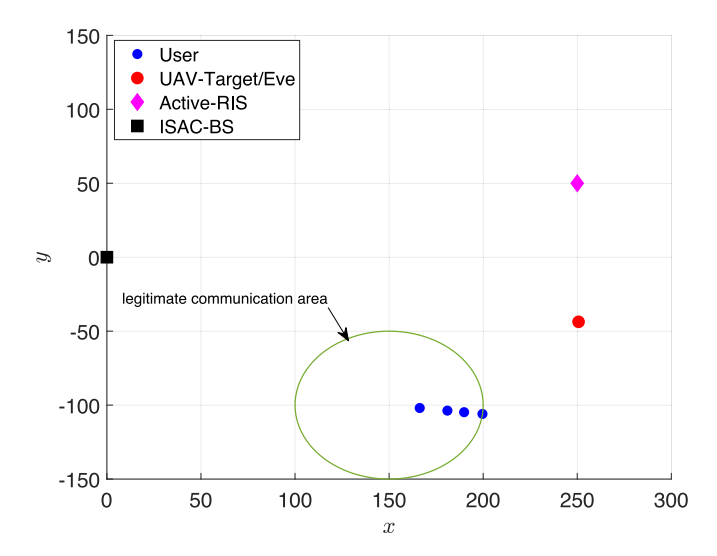


Fig. 2. A 2D instance of the proposed simulation environment.

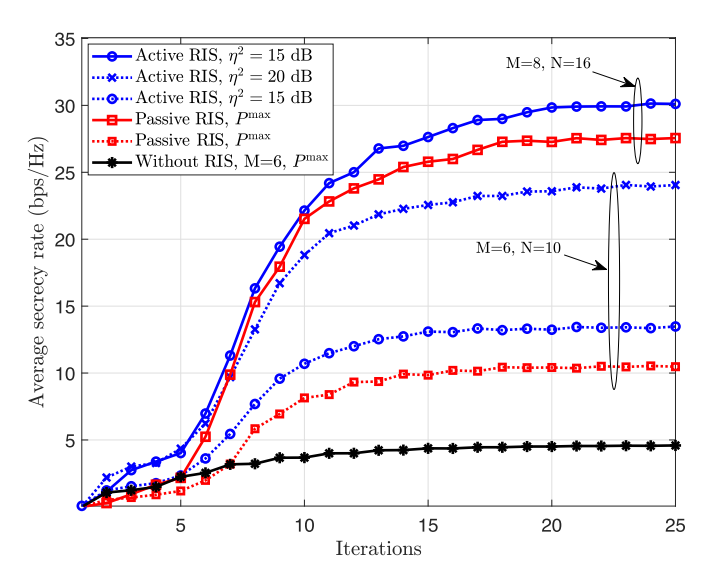


Fig. 3. Convergence of the proposed algorithm for active, passive and no RIS scenarios with different number of antenna elements and amplification factors.

RIS-user, and RIS-target links are 4, 2.5 and 2.5, respectively. Finally, the path loss models for the direct and indirect channel are set according to [40], [41] as $PL_{LOS} = -35.6 + 22 \log_{10}(d)$ and $PL_{NLOS} = 32.6 + 36.7 \log_{10}(d)$. In the following discussions, we compare the secrecy performance of the proposed active RIS-based ISAC system against the passive RIS-assisted scenario. To produce these results, the constraint in (15e) is modified to become $|\Phi(n,n)| \leq 1$ since no amplification is provided, while the constraint in (15d) is completely omitted.

Fig. 3 exhibits the convergence of the proposed Algorithm 1 for the case of active and passive RIS as well as without RIS for different number of antennas/RIS elements and active RIS amplification powers. The power budget in the active RIS scheme is $P_o = 3.16$ W at the BS and $P_I = 3.16$ W at the active RIS. For fair comparison with the passive-RIS assisted scenario, the total power budget at the BS in that case is assumed to be $P^{\max} = P_o + P_I$. As clearly shown, convergence is achieved in

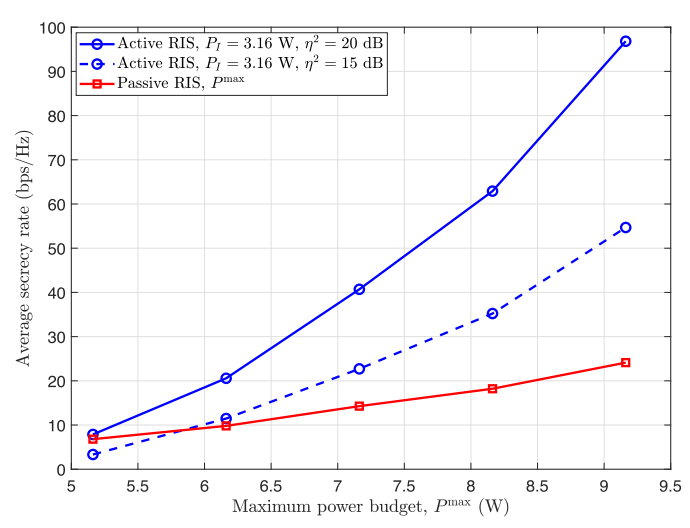
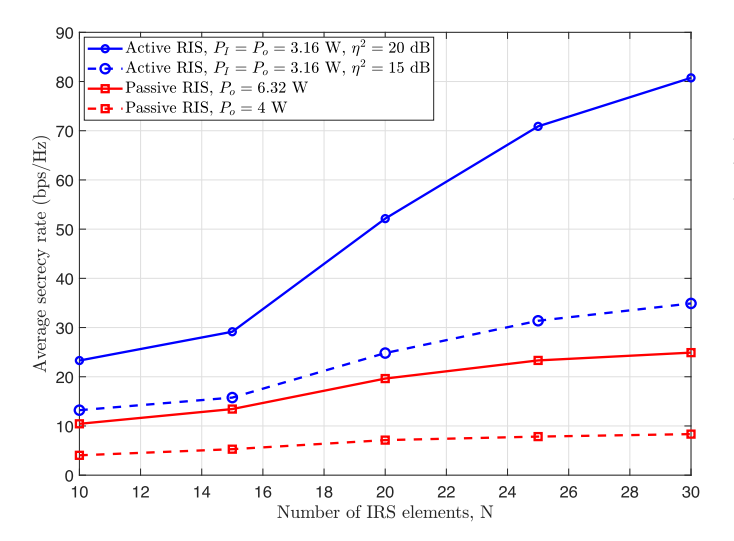


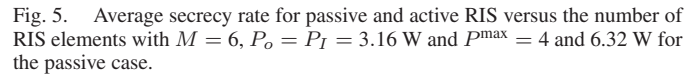
Fig. 4. Average secrecy rate versus the total power budget for passive and active RIS with M=6 and N=10 and different amplification factors.

a reasonable number of iterations for different values of M, Nand η^2 . Also, the active RIS-assisted scenario outperforms the passive one by 26.8% for M=6 and N=10 and by 9% for M=8 and N=16, both for $\eta^2=15$ dB. The reason for the reduction in the performance gap is due to the fixed power budget in the two cases despite the increase in the degrees of freedom $(DoFs)^3$ in the M=8 and N=16 case. Just like the increase in M and N provides a significant performance improvement for both the active and passive RIS cases, the amplification factor plays a vital role as well. Specifically, a significant performance improvement is observed at $\eta^2 = 20$ dB compared with the $\eta^2 = 15$ dB case for M = 6 and N = 10. Consequently, the secrecy rate of the active RIS-assisted ISAC is not only controlled by N and M but also by the amplification capability of the active elements, which could provide a multifold of performance enhancement compared with the passive RIS.

The average secrecy rate performance improvement when increasing the total power budget for the passive and active RIS with M = 6, N = 10 and different amplification factors is demonstrated next in Fig. 4. Compared to the optimal solution for the passive RIS, the secrecy rate of the active RIS-enabled system achieves a much better performance. Specifically, at 7 W maximum power budget and $\eta^2 = 15$ dB, the secrecy rate of the active RIS is about 58% better than that of the passive RIS case. Moreover, the improvement in the secrecy rate exponentially increases with ramping up the power budget. This indicates that active RIS has the potential of mitigating the "multiplicative pathloss" effect encountered in passive RIS. In addition, active RIS also guarantee low information leakage to the malicious UAV, resulting in a more secure operation at the cost of extra power consumed at its side. In other words, the constraint (15e) has a dominant effect on improving the secrecy performance, which explains the gap between the case of $\eta^2 = 20$ dB and the other cases. We also note that the passive RIS-based solution

³DoFs are defined as the maximum number of beams that can be transmitted from the base station, which is equal to the number of BS antennas.





shows slight improvement over the active RIS with $\eta^2=15~\mathrm{dB}$ at low power budgets. For example, at the first point of the curve (where $P^{\mathrm{max}}=5.16~\mathrm{W}$), the power of the active RIS scenario is distributed as $P_o=2~\mathrm{W}$ and $P_I=3.16~\mathrm{W}$, which implies that $P_o< P_I$ and hence, $\|\mathbf{\Phi}\mathbf{H}_{b,r}\mathbf{w}_i\|^2+\sigma_e^2\|\mathbf{\Phi}\|^2\geq \|\mathbf{W}\|_F^2$. In other words, the BS power transmission constraint (15c) will always be inactive. On the contrary, in the case of passive RIS, this constraint is always active and dominant, where the total power budget $P_o=5.16~\mathrm{W}$ is only available at the BS.

In Fig. 5, we evaluate the effect of increasing the number of RIS elements on the average secrecy rate for active and passive RIS with M = 6, $P_o = P_I = 3.16$ W and $P^{\text{max}} = 6.32$ and 4 W for the passive case. It is clear that the secrecy rate achieved by both the active and passive RIS cases increases with N due to increasing the DoF. Moreover, the proposed algorithm achieves a significant performance improvement compared to the existing conventional solution. Specifically, due to the impact of the "multiplicative pathloss" in the passive RIS case, the secrecy rate with $P^{\text{max}} = 6.32$ is increased by 14.5 bps/Hz when N increases from 10 to 30, which is less than the 21.8 bps/Hz increase achieved by the active RIS case at $\eta^2 = 15$ dB. However, using a larger number of elements, it is possible for passive RIS to outperform active ones using the same power budget. For example, when N=20 and $P^{\max}=6.32$, the secrecy rate of passive RIS is 19.6 bps/Hz, which is higher than that of the active RIS at $\eta^2 = 15$ dB achieving 13.2 and 15.7 bps/Hz at N=10 and N=15, respectively, However, if P^{max} is reduced to 4 W, a massive array of passive elements will have to be used to approach the secrecy performance achieved by the active RIS. Consequently, a trade-off exists between both passive and active RIS where the same secrecy rate could be achieved by either system at the same power expenditure but with large array sizes in case of the passive scenario, which could be a cheaper solution or with fewer elements in the case of the active scenario with less complex reflection coefficients matrix design.

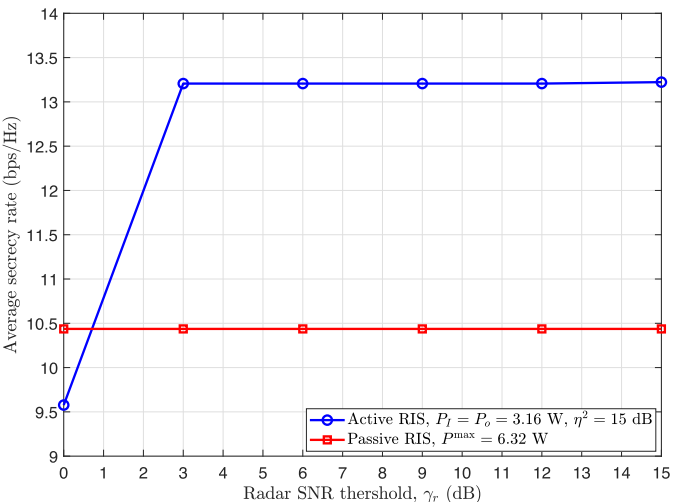


Fig. 6. Average secrecy rate versus the radar SNR threshold at $M=6,\,N=10,\,P_0=P_I=3.16$ W and $P^{\rm max}=6.32$ W.

The effect of varying the radar SNR threshold on the average secrecy rate for the passive and active RIS systems is depicted in Fig. 6 for the same power budget. As clearly seen, the active RIS exhibits an improved performance compared with the passive case, which suffers a loss of about 26.8%, again due to the "double fading effect". Furthermore, the secrecy rate in the passive case is generally constant regardless of the value of γ_r , since constraint (15b) is always inactive when compared to the power constraints (15c) and (15d). The constant behavior of the secrecy rate in Fig. 6 can be explained as follows. We first note that the radar SNR in (15b) is lower bounded by the threshold γ_r . In addition, the power constraints in (15c) and (15d) limit the secrecy performance by setting upper bounds on the transmission power. At a first glance, one might think that the secrecy performance should improve with the increase in the radar SNR threshold due to enhancing the ability of revealing the existence of the eavesdropper and hence, disrupting their data interception. However, increasing γ_r also implies more power allocation in the transmit beamformers, as shown by (15b), which would increase the probability of data interception at the target, which, in turn, could lead to a significant deterioration in secrecy rate. Hence, keeping the secrecy performance at a fixed value with increasing γ_r seems to be the optimal solution resulting from optimizing both ϕ and W, which would maintain the target detection without sacrificing the secrecy performance. It is noticeable that the passive RIS with $\gamma_r \leq 1$ dB provides a 1 bps/Hz rate improvement over the active-based system, since constraint (15c), $\|\mathbf{W}\|_F^2 \leq P^{\max}$, overrides the others, which implies that in this case, $\mathrm{SNR}_{\mathrm{rad}} \leq 1~\mathrm{dB}$ and $|\phi| \leq 1$.

In Fig. 7, we plot an example of the optimal transmit beamformers pattern gain versus the angular direction $[-90^{\circ}, 90^{\circ}]$ obtained by evaluating $\Gamma(\theta, \mathbf{W}) = \mathbf{a}^H(\theta)\mathbf{W}\mathbf{W}^H\mathbf{a}(\theta)$ for a single Monte Carlo realization. It is well-known that the DoF of the dual-transmit beamformers is determined by the rank of the covariance matrix of W, R_W , which should be larger than the number of users [42]. Numerically solving the optimization problem using CVX for this simulation instance reveals that the

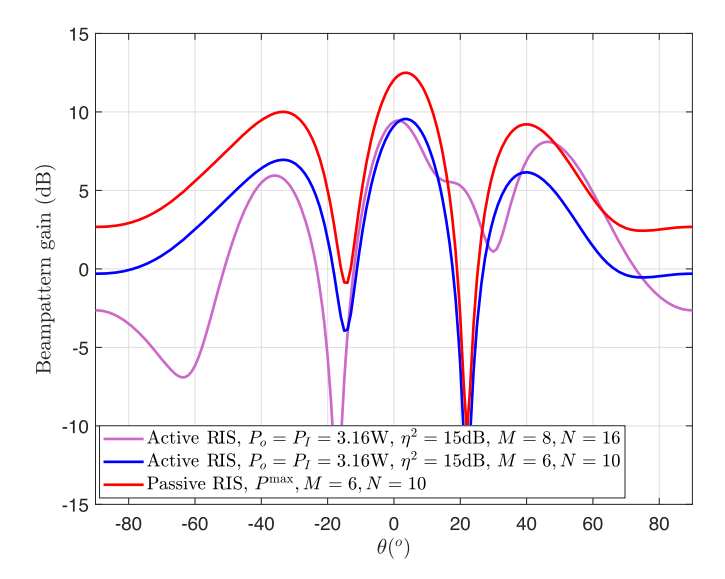


Fig. 7. Transmit beamformers pattern gain versus angular direction for passive and active RIS cases with $P^{\max}=6.32$ W.

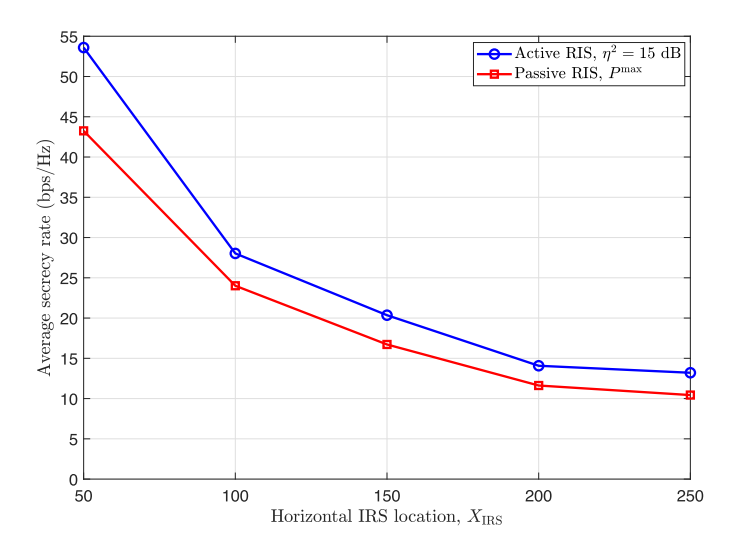


Fig. 8. Average secrecy rate versus the horizontal distance of the RIS from the BS at M=6, N=10, $P_o=P_I=3.16$ W and $P^{\rm max}=6.32$ W.

rank of R_W is 5, which means that the DoF is 5 with optimal secrecy performance. The proposed algorithm thus achieves 5 DoF for 4 communication users and one target (which is treated as a virtual downlink user). Hence, the active and passive-based ISAC systems both achieve a beamformer pattern, which meets the constraints of both the communication and radar components when M=6 and K=4. The passive RIS beam pattern has a higher gain in the synthesized beam compared with the active case though, which is quite expected due to the availability of the total power budget P^{\max} at the BS.

Finally, Fig. 8 depicts the behavior of the secrecy rate versus the change in the RIS horizontal distance from the BS, see Fig. 2. As the distance between the BS and RIS increases, the secrecy performance decays. This can be attributed to the increase in the large scale pathloss of the BS-RIS link when the RIS is positioned away from the BS. Moreover, moving the RIS closer

to the users might help in some information leakage towards the malicious UAV, which leads to the secrecy rate decay. Choosing an active RIS still provides a better secrecy rate than the passive case though at the same power budget.

V. CONCLUSION

In this paper, optimum dual transmit beamformers, radar receiver beamformers and reflection coefficients matrix of an active RIS has been found in an active-RIS assisted MISO ISAC for secure operation where a malicious UAV is trying to intercept users' data. Specifically, the secrecy rate of the system was maximized by exploiting the potential of active RIS while taking into account the detection performance of the ISAC radar component and the total power budget. To solve this problem, FP and MM have been adopted to develop an alternating optimization algorithm that can be easily solved using standard convex optimization algorithms. Simulation results show the effectiveness of the active RIS in enhancing the secrecy performance compared to existing conventional techniques. Moreover, the proposed system does not require designing any additional artificial noise and also provides immunity against the "double fading" effect, which improves both the sensing and communication functionalities. The results also show that the secrecy performance of the active RIS can be achieved by the passive ones but with a larger number of array elements especially if a lower power budget is available.

APPENDIX A SECRECY RATE OBJECTIVE AS A FUNCTION OF W

The first term of the objective function in (17) is given by

$$R_{c} = \sum_{k=1}^{K} \log_{2} \left(1 + \frac{\|\mathbf{h}_{br,k}(\mathbf{\Phi})\mathbf{w}_{k}\|^{2}}{\sum_{j=1,j\neq k}^{K+M} \|\mathbf{h}_{br,k}(\mathbf{\Phi})\mathbf{w}_{j}\|^{2} + \sigma_{e}^{2} \|\mathbf{h}_{r,k}^{H}\mathbf{\Phi}\|^{2} + \sigma^{2}} \right).$$
(36)

By exploiting FP [37], (36) can be converted to a polynomial expression by introducing the auxiliary variables $[\gamma_1, \ldots, \gamma_K]$. Hence, the Lagrangian dual expression of (36) is given by

$$R_{c} = \sum_{k=1}^{K} \log_{2} (1 + \gamma_{k}) - \sum_{k=1}^{K} \gamma_{k} + \sum_{k=1}^{K} \frac{(1 + \gamma_{k}) \left| \mathbf{h}_{br,k} \left(\mathbf{\Phi} \right) \mathbf{w}_{k} \right|^{2}}{\sum_{j=1, j \neq k}^{K+M} \left| \mathbf{h}_{br,k} \left(\mathbf{\Phi} \right) \mathbf{w}_{j} \right|^{2} + \sigma_{e}^{2} \left\| \mathbf{h}_{r,k}^{H} \mathbf{\Phi} \right\|^{2} + \sigma^{2}},$$
(37)

in which the optimization variable W is extracted out from the log function. We observe that the third term in (37) is still in fractional form, hence, we re-invoke FP and introduce additional auxiliary variables $[c_1,\ldots,c_K]$ to convert it into a polynomial expression to yield

$$R_{c} = \sum_{k=1}^{K} \log_{2} (1 + \gamma_{k}) - \sum_{k=1}^{K} \gamma_{k} - \sum_{k=1}^{K} |c_{k}|^{2} \left(\sigma^{2} - \sigma_{e}^{2} \|\mathbf{h}_{r,k}^{H} \mathbf{\Phi}\|^{2}\right)$$

$$+2\sum_{k=1}^{K}\sqrt{1+\gamma_{k}}\Re\left\{c_{k}^{*}\mathbf{h}_{br,k}\left(\mathbf{\Phi}\right)\mathbf{w}_{k}\right\}$$

$$-\sum_{k=1}^{K}\left|c_{k}\right|^{2}\sum_{j=1,j\neq k}^{K+M}\left|\mathbf{h}_{br,k}\left(\mathbf{\Phi}\right)\mathbf{w}_{j}\right|^{2}.$$
(38)

Assuming all the other variables are fixed, the auxiliary variables are calculated by differentiating (38) with respect to γ_k and c_k and setting the result to zero yielding

$$\gamma_{k} = \frac{\left|\mathbf{h}_{br,k}\left(\mathbf{\Phi}\right)\mathbf{w}_{k}\right|^{2}}{\sum_{j=1,j\neq k}^{K+M}\left|\mathbf{h}_{br,k}\left(\mathbf{\Phi}\right)\mathbf{w}_{j}\right|^{2} + \sigma_{e}^{2}\left\|\mathbf{h}_{r,k}^{H}\mathbf{\Phi}\right\|^{2} + \sigma^{2}},$$
 (39)

$$c_{k} = \frac{\sqrt{1 + \gamma_{k}} \mathbf{h}_{br,k} \left(\mathbf{\Phi}\right) \mathbf{w}_{k}}{\sum_{j=1, j \neq k}^{K+M} \left|\mathbf{h}_{br,k} \left(\mathbf{\Phi}\right) \mathbf{w}_{j}\right|^{2} + \sigma_{e}^{2} \left\|\mathbf{h}_{r,k}^{H} \mathbf{\Phi}\right\|^{2} + \sigma^{2}}.$$
 (40)

We observe that \mathbf{w}_j can be written in terms of $\tilde{\mathbf{w}}$ as $\mathbf{w}_j = \Pi_j \tilde{\mathbf{w}}$, where $\Pi_j \in \mathbb{C}^{M \times M(K+M)}$ refers to a permutation matrix, which reconstructs \mathbf{w}_j from $\tilde{\mathbf{w}}$. By defining $\ddot{\mathbf{a}}$, $\ddot{\mathbf{B}}$ and $\mathbf{b}_{k,j}$ as follows

$$\ddot{\mathbf{a}} \triangleq \left[2c_{1}^{*}\sqrt{1+\gamma_{1}}\mathbf{h}_{br,1}\left(\Phi\right),\ldots,2c_{K}^{*}\sqrt{1+\gamma_{K}}\mathbf{h}_{br,K}\left(\Phi\right),\right.$$

$$\mathbf{0}_{1 \times M(K+M) - MK} \Big]^H \in \mathbb{C}^{M(K+M) \times 1}, \tag{41}$$

$$\ddot{\mathbf{B}} = [\mathbf{b}_{1,1}, \dots, \mathbf{b}_{K,K+M}]^{\mathrm{T}} \in \mathbb{C}^{(K+M) \times M(K+M)}, \tag{42}$$

$$\mathbf{b}_{k,j} \triangleq |c_k| \, \Pi_j^T \mathbf{h}_{br,k}^H \in \mathbb{C}^{M(K+M) \times 1}, \tag{43}$$

one can write the sum rate of all legitimate devices as a function of the DRC-BF as

$$R_{c} = \varepsilon_{1} + 2\sum_{k=1}^{K} \sqrt{1 + \gamma_{k}} \Re \left\{ c_{k}^{*} \mathbf{h}_{br,k} \left(\mathbf{\Phi} \right) \mathbf{w}_{k} \right\}$$

$$- \sum_{k=1}^{K} \left| c_{k} \right|^{2} \sum_{j=1, j \neq k}^{K+M} \left| \mathbf{h}_{br,k} \left(\mathbf{\Phi} \right) \mathbf{w}_{j} \right|^{2}$$

$$= \varepsilon_{1} + \Re \left\{ \ddot{\mathbf{a}}^{H} \tilde{\mathbf{w}} \right\} - \left\| \ddot{\mathbf{B}} \tilde{\mathbf{w}} \right\|^{2}, \tag{44}$$

Similarly, the data rate at the malicious UAV is given in polynomial form as

$$R_{u} = \underbrace{\log_{2}\left(1 + \gamma_{u}\right) - \gamma_{u} - \left|c_{u}\right|^{2} \sigma^{2} - \left|c_{u}\right|^{2} \sigma_{e}^{2} \left\|\mathbf{h}_{r,t}^{H} \mathbf{\Phi}\right\|^{2}}_{\varepsilon_{2}} + 2\sqrt{1 + \gamma_{u}} \Re \left\{c_{u}^{*} \sum_{i=1}^{K+M} \mathbf{h}_{br,u} \left(\mathbf{\Phi}\right) \mathbf{w}_{i}\right\},$$
(45)

wherein the auxiliary variables are similarly defined as

$$\gamma_{u} = \frac{\sum_{i=1}^{K+M} \left| \mathbf{h}_{br,u} \left(\mathbf{\Phi} \right) \mathbf{w}_{i} \right|^{2}}{\sigma_{e}^{2} \left\| \mathbf{h}_{r,t}^{H} \mathbf{\Phi} \right\|^{2} + \sigma^{2}}, \tag{46}$$

$$c_{u} = \frac{\sqrt{1 + \gamma_{u}} \sum_{i=1}^{K+M} \mathbf{h}_{br,u} \left(\mathbf{\Phi}\right) \mathbf{w}_{i}}{\sigma_{e}^{2} \left\|\mathbf{h}_{r,t}^{H} \mathbf{\Phi}\right\|^{2} + \sigma^{2}}.$$
 (47)

Defining \mathbf{a}_{u} as

$$\mathbf{a}_{u} \triangleq \left[2c_{u}^{*}\sqrt{1+\gamma_{u}}\mathbf{h}_{br,u}\left(\Phi\right),\ldots,2c_{u}^{*}\sqrt{1+\gamma_{u}}\mathbf{h}_{br,u}\left(\Phi\right)\right]^{H},\tag{48}$$

the achievable UAV rate of (45) is rewritten as

$$R_u = \varepsilon_2 + \Re \left\{ \mathbf{a}_u^H \tilde{\mathbf{w}} \right\}. \tag{49}$$

By subtracting (49) from (44), the result in (18) can be obtained, where

$$\varepsilon = \varepsilon_1 - \varepsilon_2,\tag{50}$$

$$\mathbf{a} = \ddot{\mathbf{a}} - \mathbf{a}_u. \tag{51}$$

APPENDIX B

SECRECY RATE OBJECTIVE AS A FUNCTION ϕ

Observing that $\mathbf{h}_{br,k}(\mathbf{\Phi})\mathbf{w}_k = (\mathbf{h}_{b,k}^H + \mathbf{h}_{r,k}^H \mathbf{\Phi} \mathbf{H}_{b,r})\mathbf{w}_k = \mathbf{h}_{b,k}^H \mathbf{w}_k + \mathbf{h}_{r,k}^H \mathrm{diag}\{\mathbf{H}_{b,r}\mathbf{w}_k\}\boldsymbol{\phi}$, one can write the second term in the result of Lemma 1 as

$$\ddot{\mathbf{a}}^{H}\tilde{\mathbf{w}} = \sum_{k=1}^{K} \left(2c_{k}\sqrt{1 + \gamma_{k}} \operatorname{diag}\left\{\mathbf{w}_{k}^{H}\mathbf{H}_{br}^{H}\right\} \mathbf{h}_{r,k} \right)^{H} \boldsymbol{\phi}$$

$$+ 2\sum_{k=1}^{K} c_{k}^{*}\sqrt{1 + \gamma_{k}} \mathbf{h}_{b,k}^{H} \mathbf{w}_{k}, \tag{52}$$

while the third term becomes

$$\left\|\ddot{\mathbf{B}}\tilde{\mathbf{w}}\right\|^{2} = \sum_{k=1}^{K} \left|c_{k}\right|^{2} \sum_{j=1}^{K+M} \left|\mathbf{h}_{b,k}^{H} \mathbf{w}_{j}\right|^{2}$$

$$+ \sum_{k=1}^{K} \left(2\Re\left\{\left|c_{k}\right|^{2} \sum_{j=1}^{K+M} \operatorname{diag}\left\{\mathbf{w}_{j}^{H} \mathbf{H}_{br}^{H}\right\} \mathbf{h}_{r,k}^{*} \mathbf{h}_{b,k}^{T} \mathbf{w}_{j}\right\}\right) \boldsymbol{\phi}$$

$$+ \sum_{k=1}^{K} \boldsymbol{\phi}^{H} \left(\left|c_{k}\right|^{2} \sum_{j=1}^{K+M} \operatorname{diag}\left\{\mathbf{w}_{j}^{H} \mathbf{H}_{br}^{H}\right\} \mathbf{h}_{r,k}^{*} \mathbf{h}_{r,k}^{T} \operatorname{diag}\left\{\mathbf{H}_{b,r} \mathbf{w}_{j}\right\}\right) \boldsymbol{\phi}$$
(53)

Substituting (52) and (53) into (18) and arranging the result, we obtain the total sum rate of legitimate devices as an explicit function of ϕ as

$$R_{c} = \varepsilon_{3} + \Re \left\{ \ddot{\mathbf{a}}^{H} \boldsymbol{\phi} \right\} - \boldsymbol{\phi}^{H} \left(\ddot{\mathbf{B}} + \bar{\mathbf{H}}_{r,k} \right) \boldsymbol{\phi}, \tag{54}$$

where

$$\begin{split} \ddot{\mathbf{a}} &= 2\sum_{k=1}^{K} c_k \sqrt{1 + \gamma_k} \mathrm{diag} \left\{ \mathbf{w}_k^H \mathbf{H}_{br}^H \right\} \mathbf{h}_{r,k} \\ &- 2\sum_{k=1}^{K} |c_k|^2 \sum_{j=1}^{K+M} \mathrm{diag} \left\{ \mathbf{w}_j^H \mathbf{H}_{br}^H \right\} \mathbf{h}_{r,k} \mathbf{h}_{b,k}^H \mathbf{w}_j \end{split}$$

$$\ddot{\mathbf{B}} = \sum_{k=1}^{K} \left| c_k \right|^2 \sum_{j=1}^{K+M} \operatorname{diag} \left\{ \mathbf{w}_j^H \mathbf{H}_{br}^H \right\} \mathbf{h}_{r,k} \mathbf{h}_{r,k}^H \operatorname{diag} \left\{ \mathbf{H}_{b,r} \mathbf{w}_j \right\},$$

(47)
$$\bar{\mathbf{H}}_{r,k} = \sum_{k=1}^{K} |c_k|^2 \sigma_e^2 \operatorname{diag}\left\{\mathbf{h}_{r,k}^H\right\} \operatorname{diag}\left\{\mathbf{h}_{r,k}\right\},$$

$$\varepsilon_{3} = \sum_{k=1}^{K} \log_{2} (1 + \gamma_{k}) - \sum_{k=1}^{K} \gamma_{k} - \sum_{k=1}^{K} |c_{k}|^{2} \sigma^{2}$$

$$+ \sum_{k=1}^{K} \left(2\sqrt{1 + \gamma_{k}} \Re \left\{ c_{k}^{*} \mathbf{h}_{b,k}^{H} \mathbf{w}_{k} \right\} - |c_{k}|^{2} \sum_{j=1}^{K+M} \left| \mathbf{h}_{b,k}^{H} \mathbf{w}_{j} \right|^{2} \right),$$

Similarly, the aggregated data rate at the UAV becomes

$$\begin{split} R_{u} &= \varepsilon_{4} - \left|c_{u}\right|^{2} \sigma_{e}^{2} \boldsymbol{\phi}^{H} \operatorname{diag}\left\{\mathbf{h}_{r,t}^{H}\right\} \operatorname{diag}\left\{\mathbf{h}_{r,t}\right\} \boldsymbol{\phi} \\ &+ \Re\left\{\left(2c_{u} \sqrt{1 + \gamma_{u}} \sum_{i=1}^{K+M} \operatorname{diag}\left\{\mathbf{w}_{i}^{H} \mathbf{H}_{br}^{H}\right\} \mathbf{h}_{r,t}\right)^{H} \boldsymbol{\phi}\right\} \end{split}$$

$$= \varepsilon_4 - \boldsymbol{\phi}^H \bar{\mathbf{H}}_{r,t} \boldsymbol{\phi} + \Re \left\{ \bar{\mathbf{a}}_u^H \boldsymbol{\phi} \right\}, \tag{55}$$

where

$$\begin{split} \mathbf{\bar{a}}_{u} &= 2c_{u}\sqrt{1 + \gamma_{u}} \sum_{i=1}^{K+M} \operatorname{diag}\left\{\mathbf{w}_{i}^{H} \mathbf{H}_{br}^{H}\right\} \mathbf{h}_{r,t}, \\ \varepsilon_{4} &= \log_{2}\left(1 + \gamma_{u}\right) - \gamma_{u} - \left|c_{u}\right|^{2} \sigma^{2}, \\ &+ \Re\left\{2c_{u}^{*} \sqrt{1 + \gamma_{u}} \sum_{i=1}^{K+M} \mathbf{h}_{b,t}^{H} \mathbf{w}_{i}\right\}, \end{split}$$

$$\bar{\mathbf{H}}_{r,t} = \left| c_u \right|^2 \sigma_e^2 \operatorname{diag} \left\{ \mathbf{h}_{r,t}^H \right\} \operatorname{diag} \left\{ \mathbf{h}_{r,t} \right\}.$$

Finally, substituting (54) and (55) into (18) yields the result in (24), where

$$\mathbf{v} = \ddot{\mathbf{a}} - \bar{\mathbf{a}}_u,\tag{56}$$

$$\mathbf{Q} = \ddot{\mathbf{B}} + \bar{\mathbf{H}}_{r,k} - \bar{\mathbf{H}}_{r,t},\tag{57}$$

$$\bar{\varepsilon} = \varepsilon_3 - \varepsilon_4. \tag{58}$$

REFERENCES

- P. Brown, "75.4 billion devices connected to the Internet of Things by 2025," *Electronics*, vol. 360, 2016. Accessed: Dec. 10, 2022. [Online]. Available: https://electronics360.globalspec.com/article/6551/75-4-billion-devices-connected-to-the-internet-of-things-by-2025
- [2] K. B. Letaief, W. Chen, Y. Shi, J. Zhang, and Y.-J. A. Zhang, "The roadmap to 6G: AI empowered wireless networks," *IEEE Commun. Mag.*, vol. 57, no. 8, pp. 84–90, Aug. 2019.
- [3] W. Saad, M. Bennis, and M. Chen, "A vision of 6G wireless systems: Applications, trends, technologies, and open research problems," *IEEE Netw.*, vol. 34, no. 3, pp. 134–142, May/Jun. 2020.
- [4] M. Kafafy, A. S. Ibrahim, and M. H. Ismail, "Optimal placement of reconfigurable intelligent surfaces for spectrum coexistence with radars," *IEEE Trans. Veh. Technol.*, vol. 71, no. 6, pp. 6574–6585, Jun. 2022.
- [5] J. A. Zhang et al., "Enabling joint communication and radar sensing in mobile networks—A survey," *IEEE Commun. Surveys Tuts.*, vol. 24, no. 1, pp. 306–345, Jan.—Mar. 2021.
- [6] F. Liu et al., "Integrated sensing and communications: Towards dual-functional wireless networks for 6G and beyond," *IEEE J. Sel. Areas Commun.*, vol. 40, no. 6, pp. 1728–1767, Jun. 2022.
- [7] Z. Ren, L. Qiu, and J. Xu, "Optimal transmit beamforming for secrecy integrated sensing and communication," in *Proc. IEEE Int. Conf. Commun.*, 2021, pp. 5555–5560.
- [8] F. Liu, L. Zhou, C. Masouros, A. Li, W. Luo, and A. Petropulu, "To-ward dual-functional radar-communication systems: Optimal waveform design," *IEEE Trans. Signal Process.*, vol. 66, no. 16, pp. 4264–4279, Aug. 2018

- [9] F. Liu, C. Masouros, A. Li, J. Zhou, and L. Hanzo, "Simultaneous target detection and multi-user communications enabled by joint beamforming," in *Proc. IEEE Radar Conf.*, 2018, pp. 0089–0094.
- [10] A. Liu et al., "A survey on fundamental limits of integrated sensing and communication," *IEEE Commun. Surveys Tuts.*, vol. 24, no. 2, pp. 994–1034, Apr.–Jun. 2022.
- [11] D. K. P. Tan et al., "Integrated sensing and communication in 6G: Motivations, use cases, requirements, challenges and future directions," in *Proc. 1st IEEE Int. Online Symp. Joint Commun. Sens.*, 2021, pp. 1–6.
- [12] H. Hua, J. Xu, and T. X. Han, "Optimal transmit beamforming for integrated sensing and communication," 2021, arXiv:2104.11871.
- [13] C. Huang et al., "Holographic MIMO surfaces for 6G wireless networks: Opportunities, challenges, and trends," *IEEE Wireless Commun.*, vol. 27, no. 5, pp. 118–125, Oct. 2020.
- [14] L. Wei et al., "Multi-user holographic MIMO surfaces: Channel modeling and spectral efficiency analysis," *IEEE J. Sel. Topics Signal Process.*, vol. 16, no. 5, pp. 1112–1124, Aug. 2022.
- [15] Q. Wu, S. Zhang, B. Zheng, C. You, and R. Zhang, "Intelligent reflecting surface-aided wireless communications: A tutorial," *IEEE Trans. Commun.*, vol. 69, no. 5, pp. 3313–3351, May 2021.
- [16] M. Di Renzo et al., "Smart radio environments empowered by reconfigurable intelligent surfaces: How it works, state of research, and the road ahead," *IEEE J. Sel. Areas Commun.*, vol. 38, no. 11, pp. 2450–2525, Nov. 2020.
- [17] Z. Zhang et al., "Active RIS vs. passive RIS: Which will prevail in 6G?," 2021, arXiv:2103.15154.
- [18] J. Xu et al., "Reconfiguring wireless environment via intelligent surfaces for 6G: Reflection, modulation, and security," 2022, arXiv:2208.10931.
- [19] K. Zhi, C. Pan, H. Ren, K. K. Chai, and M. Elkashlan, "Active RIS versus passive RIS: Which is superior with the same power budget?," *IEEE Commun. Lett.*, vol. 26, no. 5, pp. 1150–1154, May 2022.
- [20] M. Najafi, V. Jamali, R. Schober, and H. V. Poor, "Physics-based modeling and scalable optimization of large intelligent reflecting surfaces," *IEEE Trans. Commun.*, vol. 69, no. 4, pp. 2673–2691, Apr. 2021.
- [21] L. Dong, H.-M. Wang, and J. Bai, "Active reconfigurable intelligent surface aided secure transmission," *IEEE Trans. Veh. Technol.*, vol. 71, no. 2, pp. 2181–2186, Feb. 2022.
- [22] X. Tong et al., "Environment sensing considering the occlusion effect: A multi-view approach," *IEEE Trans. Signal Process.*, vol. 70, pp. 3598–3615, 2022.
- [23] X. Tong, Z. Zhang, J. Wang, C. Huang, and M. Debbah, "Joint multi-user communication and sensing exploiting both signal and environment sparsity," *IEEE J. Sel. Topics Signal Process.*, vol. 15, no. 6, pp. 1409–1422, Nov. 2021.
- [24] H. Luo, R. Liu, M. Li, Y. Liu, and Q. Liu, "Joint beamforming design for RIS-assisted integrated sensing and communication systems," *IEEE Trans. Veh. Technol.*, early access, Aug. 09, 2022, doi: 10.1109/TVT.2022.3197448.
- [25] F. Liu, C. Masouros, A. P. Petropulu, H. Griffiths, and L. Hanzo, "Joint radar and communication design: Applications, State-of-the-Art, and the road ahead," *IEEE Trans. Commun.*, vol. 68, no. 6, pp. 3834–3862, Jun. 2020.
- [26] X. Song, D. Zhao, H. Hua, T. X. Han, X. Yang, and J. Xu, "Joint transmit and reflective beamforming for IRS-assisted integrated sensing and communication," in *Proc. IEEE Wireless Commun. Netw. Conf.*, 2022, pp. 189–194.
- [27] R. Liu, M. Li, Y. Liu, Q. Wu, and Q. Liu, "Joint transmit waveform and passive beamforming design for RIS-aided DFRC systems," *IEEE J. Sel. Topics Signal Process.*, vol. 16, no. 5, pp. 995–1010, Aug. 2022.
- [28] R. Liu, M. Li, and A. L. Swindlehurst, "Joint beamforming and reflection design for RIS-assisted ISAC systems," in *Proc. 30th Eur. Signal Process.* Conf., 2022, pp. 997–1001.
- [29] R. Sankar and S. P. Chepuri, "Beamforming in hybrid RIS assisted integrated sensing and communication systems," in *Proc. 30th Eur. Signal Process. Conf.*, 2022, pp. 1082–1086.
- [30] H. Du, J. Kang, D. Niyato, J. Zhang, and D. I. Kim, "Reconfigurable intelligent surface-aided joint radar and covert communications: Fundamentals, optimization, and challenges," *IEEE Veh. Technol. Mag.*, vol. 17, no. 3, pp. 54–64, Sep. 2022.
- [31] N. Su, F. Liu, Z. Wei, Y.-F. Liu, and C. Masouros, "Secure dual-functional radar-communication transmission: Exploiting interference for resilience against target eavesdropping," *IEEE Trans. Wireless Commun.*, vol. 21, no. 9, pp. 7238–7252, Sep. 2022.
- [32] N. Su, F. Liu, and C. Masouros, "Secure radar-communication systems with malicious targets: Integrating radar, communications and jamming functionalities," *IEEE Trans. Wireless Commun.*, vol. 20, no. 1, pp. 83–95, Inc. 2021.

- [33] C. You and R. Zhang, "Wireless communication aided by intelligent reflecting surface: Active or passive?," *IEEE Wireless Commun. Lett.*, vol. 10, no. 12, pp. 2659–2663, Dec. 2021.
- [34] R. Long, Y.-C. Liang, Y. Pei, and E. G. Larsson, "Active reconfigurable intelligent surface-aided wireless communications," *IEEE Trans. Wireless Commun.*, vol. 20, no. 8, pp. 4962–4975, Aug. 2021.
- [35] D. Xu, X. Yu, D. W. K. Ng, and R. Schober, "Resource allocation for active irs-assisted multiuser communication systems," in *Proc. IEEE 55th Asilomar Conf. Signals, Syst., Comput.*, 2021, pp. 113–119.
- [36] J. Joung, C. K. Ho, K. Adachi, and S. Sun, "A survey on power-amplifier-centric techniques for spectrum-and energy-efficient wireless communications," *IEEE Commun. Surveys Tuts.*, vol. 17, no. 1, pp. 315–333, Jan.–Mar. 2015.
- [37] K. Shen and W. Yu, "Fractional programming for communication systems— Part I: Power control and beamforming," *IEEE Trans. Signal Process.*, vol. 66, no. 10, pp. 2616–2630, May 2018.
- [38] M. Grant, S. Boyd, and Y. Ye, "CVX: Matlab software for disciplined convex programming," 2008. [Online]. Available: http://cvxr.com/cvx/
- [39] Y. Sun, P. Babu, and D. P. Palomar, "Majorization-minimization algorithms in signal processing, communications, and machine learning," *IEEE Trans. Signal Process.*, vol. 65, no. 3, pp. 794–816, Feb. 2017.
- [40] H. Ibraiwish, A. Elzanaty, Y. H. Al-Badarneh, and M.-S. Alouini, "EMF-aware cellular networks in RIS-assisted environments," *IEEE Commun. Lett.*, vol. 26, no. 1, pp. 123–127, Jan. 2022.
- [41] "Evolved universal terrestrial radio access (E-UTRA); Further advancements for E-UTRA physical layer aspects (release 9)," ETSI Tech. Specification TS 136 300 V9.4.0, 2010.
- [42] X. Liu, T. Huang, N. Shlezinger, Y. Liu, J. Zhou, and Y. C. Eldar, "Joint transmit beamforming for multiuser MIMO communications and MIMO radar," *IEEE Trans. Signal Process.*, vol. 68, pp. 3929–3944, 2020



Mahmoud H. Ismail (Senior Member, IEEE) received the B.Sc. degree (with highest Hons.) in electronics and electrical communications engineering, the M.Sc. degree in communications engineering from Cairo University, Cairo, Egypt, in 2000 and 2002, respectively, and the Ph.D. degree in electrical engineering from The University of Mississippi, Oxford, MS, USA, in 2006. From August 2000 to August 2002, he was a Research and Teaching Assistant with the Department of Electronics and Electrical Communications Engineering, Cairo University. From 2004

to 2006, he was a Research Assistant with the Center for Wireless Communications (CWC), University of Mississippi. He is currently a Full Professor with the American University of Sharjah, Sharjah, UAE, and a Full Professor (on leave) with the Department of Electronics and Electrical Communications Engineering, Cairo University. From 2006 to 2014, he was also a Systems Engineering Consultant with Newport Media Inc. (now part of Microchip), Cairo. His research interests include wireless communications with emphasis on performance evaluation of next-generation wireless systems and communications over fading channels. He was the recipient of the University of Mississippi Summer Assistantship Award in 2004 and 2005, The University of Mississippi Dissertation Fellowship Award in 2006. The University of Mississippi Graduate Achievement Award in Electrical Engineering in 2006 and the Best Paper Award presented at the 10th IEEE Symposium on Computers and Communications (ISCC 2005), La Manga del Mar Menor, Spain.



A. Abdelaziz Salem received the M.Sc. and Ph.D. degrees in electronics and electrical communications engineering from the Faculty of Electronic Engineering, Menoufia University, Shibin Al Kawm, Egypt, in 2015 and 2019, respectively. He is currently a Post-doctoral Research Fellow with the American University of Sharjah, Sharjah, UAE. He is also an Assistant Professor with the Department of Electronics and Electrical Communications Engineering, Menoufia University. His research interests include applying convex optimization approaches on ultra-dense net-

works, vehicular communications, intelligent reflecting surface assisted communications, non-orthogonal multiple access, and game theory applications.



Ahmed S. Ibrahim (Member, IEEE) received the B.S. and M.S. degrees in electronics and electrical communications engineering from Cairo University, Cairo, Egypt, in 2002 and 2004, respectively, and the Ph.D. degree in electrical engineering from the University of Maryland, College Park, MD, USA, in 2009. He is currently an Associate Professor with the Electrical and Computer Engineering Department, Florida International University (FIU), Miami, FL, USA. He was the recipient of the NSF CAREER Award in 2022. Prior to joining FIU, he was an

Assistant Professor with Cairo University, a Wireless Research Scientist with Intel Corporation, and Senior Engineer with Interdigital Communications Inc. His research interests include various topics of wireless systems, including drone-assisted millimeter wave communications, vehicular communications, and rethinking wireless networks through the lens of Riemannian geometry.